Direct Ink Writing Of PVDF/PEG/CA Composite

Based Water Treatment Membranes

by

Abhinav Chavali

A Thesis Presented in Partial Fulfillment
of the Requirements for the Degree
Master Of Science

Approved July 2024 by the
Graduate Supervisory Committee:

Sui Yang, Chair
Kailong Jin
Cindy (Xiangjia) Li
Kenan Song

ARIZONA STATE UNIVERSITY

August 2024

ABSTRACT

This study explores the development of composite membranes using polyvinylidene fluoride (PVDF), polyethylene glycol (PEG) and cellulose acetate (CA) through Direct Ink Writing (DIW) technology for water treatment applications. PVDF membranes are renowned for their thermal stability, chemical resistance, and mechanical robustness. By integrating CA and PEG with PVDF via DIW, precise control over membrane structure and composition is achieved, leading to enhanced porosity, mechanical integrity, hydrophilicity and overall performance. Specifically, BET analysis confirmed uniform pore sizes and surface areas essential for efficient filtration, while mechanical testing demonstrated varied properties across different compositions, resulting in membranes that strike a balance between strength and flexibility. Contact angle measurements highlighted the role of CA and PEG in improving wettability and ensuring precise print fidelity, crucial for DIW applications requiring enhanced adhesion and pattern resolution. This research highlights DIW's capability to tailor membrane properties, overcoming limitations associated with traditional fabrication methods. The findings suggest that the synergistic blend of mechanical strength, porosity, and hydrophilicity achieved through optimized PVDF/PEG/CA compositions could significantly benefit industrial and environmental sectors that demand durable membrane materials with high-performance characteristics.

ACKNOWLEDGEMENTS

I express my deepest gratitude to Professor Kenan Song and Professor Sui Yang for their unwavering guidance and support throughout my research journey. Being welcomed into their research groups has been a privilege for which I am forever grateful.

Professor Song's mentorship has been fundamental to my academic growth. His encouragement during challenging times has fostered a spirit of innovation in my problem-solving approach. His emphasis on critical thinking has sharpened my analytical skills, and his diplomatic and supportive nature during research obstacles has greatly enhanced my resilience and adaptability. Under his guidance, I have come to value punctuality, critical inquiry, and a balanced approach to research challenges. Professor Yang's expert insights and meticulous attention to detail have been equally pivotal. His commitment to academic rigor has refined my analytical abilities and deepened my understanding of complex research concepts. His methodical approach to addressing intricate challenges has guided me in adopting a more disciplined and thorough research methodology. Together, Professors Song and Yang have created a nurturing environment that values critical inquiry and innovation. Their combined mentorship has broadened my academic horizons and instilled in me essential qualities that extend beyond academia. The knowledge, skills, and personal growth I have achieved under their guidance will be invaluable in my future endeavors. I deeply appreciate their support, which has been fundamental to the completion of this thesis.

I also want to thank my committee members, Professor Kailong Jin and Professor Cindy Li, for their support and suggestions, which have been crucial to the success of my thesis. Their insightful feedback and encouragement have helped me to refine my research focus and improve the quality of my work. I am grateful for their commitment to my academic progress and for the time they have dedicated to reviewing my work and providing valuable input.

Additionally, I am grateful to my colleagues Varun Kumar Thipanna, Nikhil Reddy Raagi, Abhishek Saji Kumar, and Shuai Feng for their support throughout my tenure in both labs. Their constant insights and guidance, drawn from their previous experiences and knowledge, made a significant contribution to completing this project. As seniors in the lab, they provided invaluable insights that significantly contributed to the success of my research. Their willingness to share knowledge, offer guidance, and assist me with various aspects of the project has shaped me into who I am today. Their insightful guidance also helped refine the experimental aspects and broadened the overall scope of my research. I would also like to thank my other lab mates from both labs for their collaborative spirit and collective contributions, which have enriched my research journey. Your support and positive energy have meaningfully impacted the overall research environment, creating a space where ideas flourish. Additionally, I want to specially thank Saleh Alfarhan, Yizhen Zhu, Vamsi Krishna, and Edgardo for their assistance with characterization techniques, and Arunachalam Ramananthan and Dhanush Patil for helping me with my thesis draft revision.

Lastly, I extend my heartfelt thanks to Arizona State University, whose support and resources have made all of this possible.

TABLE OF CONTENT

Page

CHAPTER

LIST OF FIGURES

LIST OF TABLES

1. INTRODUCTION

1.1 Background

Water filtration membranes are essential in various applications, providing clean and safe water by removing contaminants and impurities. [1] These membranes are categorized based on their pore size and filtration capabilities, including microfiltration (MF), ultrafiltration (UF), nanofiltration (NF), and reverse osmosis (RO). Each category serves different purposes, from removing large particles and bacteria (MF) to filtering out dissolved salts and small organic molecules[2], [3] Among these, MF membranes have the largest pore sizes, typically ranging from 0.1 to 10 micrometers. They can effectively remove suspended solids, bacteria, and other large particles from water. These membranes are often used as a pre-treatment step to protect more sensitive downstream processes, with common applications including water treatment plants and industrial wastewater treatment.[4], [5] UF membranes have smaller pore sizes, generally between 0.01 and 0.1 micrometers. They can remove bacteria, viruses, and some larger organic molecules. UF is commonly used for drinking water purification, dialysis, and processes sterilization and clarification processes. [6] NF membranes have even smaller pores, typically in the 0.001 to 0.01 micrometers range. They are effective at removing divalent ions, small organic molecules, and certain salts. NF membranes are used in water softening, desalination, and the removal of specific contaminants such as heavy metals and colorants from water.[7], [8] RO membranes have the smallest pore sizes, less than 0.001 micrometers, allowing them to remove nearly all dissolved salts, organic molecules, and other impurities. RO is

widely used for the desalination of seawater and brackish water, as well as for producing ultrapure water for industrial processes and drinking water.[4], [9].

Due to the versatile properties and efficient filtration capabilities, polymers play crucial roles in these water filtration membranes. The general types of polymer-based membranes include polyvinylidene fluoride (PVDF), polysulfone (PSF), polyethersulfone (PES), cellulose acetate (CA), and polypropylene (PP). Among them, polyvinylidene fluoride (PVDF) membranes are widely used due to their excellent chemical resistance, thermal stability, and mechanical strength.[10] They are particularly effective in ultrafiltration (UF) and microfiltration (MF) processes, making them suitable for industrial wastewater treatment and drinking water purification. polysulfone (PSF) and polyethersulfone (PES) membranes are known for their high mechanical strength and thermal stability. They are often used in ultrafiltration (UF) and nanofiltration (NF) applications to remove bacteria, viruses, and other small contaminants from water. These membranes are also resistant to a wide range of chemicals, enhancing their durability and longevity in harsh environments.[11], [12] On the other hand, cellulose acetate (CA) membranes offer high hydrophilicity and biodegradability, making them an environmentally friendly option for water filtration.[13] They are commonly used in reverse osmosis (RO) and nanofiltration (NF) processes to desalinate water and remove organic contaminants. CA membranes are also effective in applications requiring high flux and low fouling tendencies. [14], [15]polypropylene (PP) membranes are favored for their low cost, chemical resistance, and excellent mechanical properties. They are primarily used in microfiltration (MF) applications to remove suspended solids, bacteria, and other large

particles from water. PP membranes are widely used in pre-filtration stages to protect downstream processes and extend the life of more expensive membranes[16].

1.2 PVDF based Membranes

Polymer membranes are highly versatile, cost-effective, and easy to process, making them suitable for large-scale production[17], [18] offering significant advantages over other membrane types, such as ceramic or metallic membranes for scalable water treatment. Moreover, polymer membranes provide excellent chemical resistance, mechanical strength, and flexibility, which can be tailored to meet specific filtration requirements. These unique properties make polymer membranes a preferential choice for broad practical water filtration applications, from industrial wastewater treatment to household water purification systems.[19]

Among polymer membranes, PVDF has gained significant attention due to its exceptional properties of chemical resistance, thermal stability, and mechanical strength, allowing them to withstand harsh environmental conditions and aggressive chemicals commonly encountered in water treatment processes. [20], [21] Due to this bond nature, engineered semicrystalline PVDF membrane fabrication containing 59.4 wt% fluorine and 3 wt% hydrogen, offers high thermal stability, chemical resistance, and oxidant resistance, making it ideal for wastewater treatment and desalination. [22] In addition, PVDF's low extractables make it a pure polymer, suitable for biomedical and bio-separation applications. It also exhibits thermodynamic compatibility with other polymers like poly

(methyl methacrylate) (PMMA), enhancing its versatility in various blend compositions. [23], [24], [25] Commercially, PVDF is produced by emulsion or suspension polymerization using free radical initiators, forming the repeating unit –CH2–CF2–. The arrangement of CH2 and CF2 groups along the polymer chains affects PVDF's crystalline structure and properties. PVDF can crystallize into four distinct phases: α, β, γ, and δ, with the α-phase being the most common. This phase has a trans-gauche (TGTG′) conformation, alternating H and F atoms on each side of the chain.[10], [26] PVDF's crystallinity ranges from 35% to 70%, measurable by the specific volumes of its crystalline and amorphous phases. Chemically, PVDF is stable against harsh chemicals, including halogens, oxidants, inorganic acids, and various solvents. This stability is crucial for applications involving exposure to aggressive substances. Enhancing PVDF's hydrophilicity improves membrane fouling resistance, as a hydrophilic surface forms a pure water layer that prevents the adsorption of hydrophobic pollutants[27], [28], [29].

The exploration of PVDF and its advantageous characteristics sets the stage for discussing the role of CA membranes in enhancing the performance and functionality of membrane-based water treatment solutions. CA membranes, known for their high hydrophilicity and biodegradability, offer complementary benefits to PVDF membranes. By incorporating CA into PVDF-based membranes, it is possible to achieve a balance of mechanical strength, chemical resistance, and enhanced hydrophilicity, leading to improved filtration efficiency and reduced fouling.[30], [31] This combination leverages the strengths of both polymers, resulting in membranes that are not only robust and durable but also capable of maintaining high water flux and selectivity. The synergy between

PVDF and CA in composite membranes demonstrates the potential for developing advanced water treatment solutions that meet the increasing demand for clean and safe water in various industrial, commercial, and residential applications.

1.3 Overview of Membrane Manufacturing

Common membrane fabrication techniques include phase inversion, interfacial polymerization, and electrospinning. However, these traditional methods often face significant challenges in customizing membranes with precisely controlled dimension, porosity and membrane thickness [32], [33]. And the fabrication scalability of these methods set an ultimate limit for large scale water filtration applications.

Phase inversion involves the transformation of a polymer solution into a solid membrane through solvent exchange. This method is advantageous because it is relatively simple and can produce membranes with varying pore sizes and structures, making it versatile for different applications. However, phase inversion often results in heterogeneous pore structures and inconsistent membrane properties, which can compromise membrane performance. [34], [35] The lack of uniformity and fine-tuning required for high-performance applications limits its effectiveness in producing advanced filtration membranes.[36], [37] Additionally, controlling the pore size distribution and achieving consistent membrane morphology can be challenging, leading to variability in membrane quality.

Interfacial polymerization, another common technique, involves forming a thin polymer film at the interface of two immiscible liquids. This method's primary advantage

is its ability to produce thin, dense membranes with excellent selectivity, which is crucial for applications requiring high separation efficiency, such as reverse osmosis.[38], [39] However, interfacial polymerization is limited by the difficulty in controlling film thickness and uniformity. The process can be complex and sensitive to various parameters, such as reaction time, temperature, and concentration of reactants, making it challenging to achieve consistent results. Moreover, the interfacial polymerization process often requires the use of potentially hazardous chemicals, posing environmental and safety concerns[40], [41].

Electrospinning is a technique that uses an electric field to draw polymer fibers from a solution, creating highly porous membranes with fine fiber diameters. The advantages of electrospinning include the ability to produce membranes with high surface area-to-volume ratios and tunable porosity, making them suitable for applications requiring high permeability and surface interaction, such as filtration and biomedical applications. [42], [43], [44] However, electrospun membranes often suffer from low mechanical strength and stability, limiting their practical application in water treatment. Additionally, the scalability of electrospinning for industrial production is challenging, as it requires precise control over the electrospinning parameters and can be limited by low production rates. This poses significant challenges for widespread implementation in large-scale water treatment systems[45].

Therefore, while traditional membrane fabrication methods like phase inversion, interfacial polymerization, and electrospinning have their advantages, they also face significant limitations in achieving the uniformity, consistency, and scalability required for

high-performance water treatment membranes. These challenges necessitate the exploration of alternative materials and fabrication techniques to develop advanced membranes with tailored properties for specific applications.

1.4 Overview of Membranes from Direct Ink Writing

3D printing, also known as additive manufacturing, is a transformative technology that creates three-dimensional objects layer by layer from digital models. The primary categories of 3D printing include Fused Deposition Modeling (FDM), Stereolithography (SLA), Selective Laser Sintering (SLS), and Digital Light Processing (DLP). FDM uses thermoplastic filaments, melting and depositing them layer by layer. [46], [47] SLA and DLP use photopolymer resins cured by light, while SLS employs lasers to sinter powdered materials. Each method offers unique advantages, making 3D printing versatile for applications across various industries, from prototyping to manufacturing complex parts.

3D printing methods are revolutionizing membrane fabrication by enabling the creation of highly customizable and precise membrane structures. Techniques such as Fused Deposition Modeling (FDM), Stereolithography (SLA), and Digital Light Processing (DLP) can produce membranes with tailored dimension, geometries, pore sizes and distributions, in contrast to the traditional membrane fabrication methods. Thus, the high level fabrication control of 3D-printed membranes poses great potentials for a broad spectrum of practical applications, including water treatment, gas separation, and biomedical devices. [47], [48] Particularly, 3D printed membranes offers rapid prototyping

and scalability with the capability of innovative morphological designs, provide an ideal platform for water filtration systems.

DIW, a variant of Liquid Deposition Modeling (LDM), involves the extrusion of viscoelastic ink through a fine nozzle under pressure. This versatile method accommodates a wide range of materials, including polymer-based melts, particle-based inks, and biomaterials, making it suitable for structural, electrical, biomedical, and mechanical applications.[49], [50] DIW excels in constructing intricate structures, including those with overhangs and internal voids, making it ideal for applications like biomedical lattice, interwoven, or meta-structures. Multi-material capability in DIW is achieved through multiple print heads, a single nozzle with microfluidic switching, or simultaneous printing of numerous filament arrays. [51]Additionally, DIW introduces advanced polymerization and curing mechanisms, such as frontal polymerization, which are not feasible in other 3D printing methods.

DIW process consists of three main steps: 3D modeling using Computer-Aided-Design (CAD) software, generating a 3D movement path file for the nozzle through slicing software, and the actual ink deposition. Successful DIW printing requires pressure-driven extrusion through a specified nozzle diameter at a defined flow rate. The choice of nozzle types, such as single, core-shell, or co-axial, depends on specific print requirements. The extruded material must maintain its shape, bridging gaps and acting as a mechanically sound substrate for subsequent layers. Key machine parameters, such as nozzle size and printing speed, are crucial in determining printing accuracy and resolution.

DIW-printed membranes have demonstrated diverse applications and properties, as summarized in Table 1. For instance, geopolymer-based membranes with YSZ viscosity modifiers showed high potential in water treatment, achieving high permeance and rejection efficiency for alumina particles.[52] Dehydrofluorinated PVDF (dPVDF) membranes exhibited competitive water fluxes and hydrophobicity, suitable for microfiltration.[53] PDMS/Co membranes demonstrated superhydrophobicity, effective for oily wastewater treatment, while CA/PVA/SiO2 NP membranes excelled in oil-water separation with superoleophobic characteristics.[54] As another example, a study utilizing geopolymer-based membranes with YSZ viscosity modifiers demonstrated that varying nozzle dimensions and print speeds could achieve porosities ranging from 55.6% to 68.8%, significantly higher than traditional molded specimens. These membranes showed promising results in water treatment applications, with high permeance and rejection efficiency for alumina particles. Similarly, DIW-printed dehydrofluorinated PVDF (dPVDF) membranes achieved water contact angles (WCA) of approximately 115°, indicating their hydrophobic nature, and exhibited pure water fluxes competitive with commercial PVDF membranes, making them suitable for microfiltration applications.[53], [54], [55]

Other notable examples include PDMS/Co membranes, which exhibited superhydrophobicity with WCAs around 155°, making them effective for oily wastewater treatment.[54] Additionally, CA/PVA/SiO2 NP membranes demonstrated high-efficient oil-water separation with superoleophobic characteristics and excellent stability after multiple bending cycles.[55] Another study on CSMA/GELMA/nanographene oxide

(nGO) membranes highlighted their impressive anti-fouling properties and high water permeation flux, positioning them as green and renewable options for oil-water separation.[56] Furthermore, cellulose/sodium alginate (SA) monolithic hydrogel membranes and chitin/maleic anhydride grafted β-chitin nanofiber (MACNF) membranes showed potential in environmental and biomedical applications, respectively. The former demonstrated high methylene blue removal efficiency, while the latter exhibited good mechanical properties for wound healing applications.[57] Polyether-ether-ketone (PEEK) and sodium-carboxymethyl cellulose (Na-CMC) membranes reinforced with mesoporous bioactive glass nanoparticles also showed promise in bone tissue engineering, with significant antibacterial properties and cell viability.[58]

DIW 3D printing thereby offers numerous advantages, including the ability to create complex geometries, precise control over material distribution, and the incorporation of various functional additives. These capabilities make DIW an attractive approach for developing high-performance membranes tailored to specific filtration and separation applications, thus enhancing the efficiency and effectiveness of water treatment systems.

Table 1. Study on Membrane properties and applications manufactured using DIW

Membranes	**Printing parameters**	**Porosity**	**Contact Angles measured**	**Other membrane props**	**Applications**	**Ref.**
Geopolymers YSZ: viscosity modifier	Layer Thickness: 300 µm Platform Temperature: 75°C	55.6%–68.8%, compared with 22.4% molded specimen	NA	Pure Water Permeance: 1453 L/(m²·h·bar) 1)Permeance (with 80-nm alumina particles): 1311 L/(m²·h·bar) [under TMP] 2)Rejection Efficiency: 98.4%	high-potential alternative to ceramic-based membranes in water treatment	[52]
dPVDF	DIW at Room temperature, Membranes placed in DI water bath	NA	WCA ≈ 115° PVDF membranes WCA ≈ 99°	Pure Water Flux: dPVDF membranes: ~4300 L m^{-2} h^{-1} Commercial PVDF membranes : ~6300–8100 L m^{-2} h^{-1}	MF (Microfiltration) Applications.	[53]
PDMS/Co	Curing: 95°C for 2 hours Filling Rate: 25% to 80% Filament Spacing: 1.278 mm to 0.368 mm	Pore Size: 0.2 to 0.6 mm	WCA (Water Contact angles): 155±5, approximately	Exhibited super hydrophobicity during 600 stretching releasing cycles with 50% strain and multiple irregular folding	oily waste water treatment applications	[54]
CA +PVA, +SiO2 NPs solid like a solution	Printed membranes immersed in DI water for 60 minutes at room temperature	631 ± 31 µm	WCA varied btw 16.14 ± 2.61° to 42.9 ± 1.95° OCA (Underwater Contact Angle)>150°	Separation Efficiency: 99% superoleophobicity characteristics after 50 bending cycles, demonstrating good stability and anti-fouling properties	High-efficient oil-water separation	[55]
CSMA +GELMA + nanographene oxide (nGO)	UV Photocurable Lamp: Wavelength: 365 nm Power: 500 mW/cm² Printing Temperature: 10°C, Membranes freeze-dried before use	250 to 400 µm	Underwater OCA: 146.5 ± 1.0° to 161.5 ± 1.1°	Separation Efficiency: 99.5% Anti-fouling Properties: Achieved after 20 cyclic tests in salty, acidic, or alkaline conditions Water Permeation Flux: 39,500 L $m^{-2}h^{-1}$	Green and renewable bio based membranes in oil-water separation	[56]

cellulose/sodium alginate (SA)monolithic hydrogel (CAH)	Printed Cylinder Thickness: 2.2 mm (15 layers),5.0 mm (30 layers),7.9 mm (45 layers),10.0 mm (60 layers)	Wall thickness 0.188 ± 0.068 mm (CAH), 0.226 ± 0.056 mm (CAH-MB); Channel widths 0.765 ± 0.048 mm (CAH), 0.715 ± 0.043 mm (CAH-MB)	Super hydrophilicity exhibited	MB Removal Efficiency: 91.3% to 95.1% Adsorption Capacity: 0.88 to 0.17 mg g^{-1} (CAH dosage 0.1 to 0.5 g) BET Surface Area: 84.64 m^2 g^{-1} (CAH), 97.38 m^2 g^{-1} (CAH-MB)	Can be used in the removal of methylene blue dyes in industrial and environmental applications	[57]
Chitin/ maleic anhydride grafted β-chitin nanofibers (MACNF)	Layer Height: 320 µm Scaffold Structure: 12 filaments per layer, alternating orthogonal directions, 15 layers	Micron-size pore scaffold	NA	Mechanical Properties: Young's Modulus: 42.8 ± 0.59 kPa (5 wt%), 43.8 ± 0.20 kPa (7.5 wt%), 45.3 ± 0.58 kPa (10 wt%)	Wound dressing, wound healing	[59]
polyether-ether-ketone (PEEK) +sodium-carboxymethyl cellulose (Na-CMC) +mesoporous bioactive glass (MBGNs) of Zn and Mn	Layer height= 0.3 mm Extrusion Width=0.3 mm Extrusion Speed=1.5 mm/s Nozzle & Bed Temperature=25° C Fill Density= 0.15 Fill Angle= 45°	600 ± 30 µm	50° ± 1	Bio Properties: a) Antibacterial: Inhibition zone against Staphylococcus aureus, Escherichia coli b) Angiogenesis: Significant potential in Chick CAM assay (Zn–Mn MBGNs) c)Cell Viability: 103% viability at 7 days (WST-8 assay)	bone tissue engineering, providing a customized and effective approach for faster recovery and better patient results.	[58]
chitosan - graphene oxide (CH - GO) nanocomposite hydrogels	NA	CH3GO - 0: 40% CH3GO – 5: 52%	NA		facilitates the differentiation of neuroblastoma cells	[60]
cellulose nanofibrils reinforced aloe vera bio-hydrogels	Number of Layers: 5 1)Infill Density: 100%					[61]
Notes: CA-Cellulose Acetate; CS-Chitosan ;CSMA- methacrylate chitosan ;dPVDF- dehydrofluorinated Polyvinylidene fluoride ;DIW-Direct Ink Writing ; Fluoropor- Fluorolink MD700+1H,1,2H,2H-per-fluorooctanol;FDM-Fusion Deposition Modelling ;FFF-Fused Filament Fabrication; GELMA- methacrylate gelatin; Geopolymers: metakaolin powders + sodium silicate solution + sodium hydroxide pellets; nGO-Nanographene Oxide; PDMS/Co-Polydimethylsiloxane/Cobalt; PLA-Polylactic Acid; Plastic membrane mixture: ,						

[2- (methacryloyloxy) ethyl] dimethyl-(3- sulfopropyl) ammonium hydroxide, acrylamide PVA-Polyvinyl Alcohol; SiO_2 NPs -silica nano-particles ;SLA-Stereolithography; YSZ- Yttria stabilized zirconia powders

1

1.5 Key Performance Indicators (KPI) of Membranes in this Study

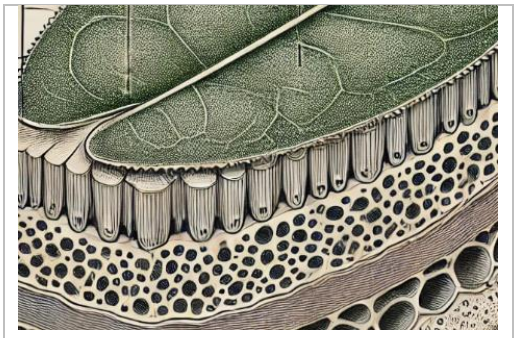

Figure 1. Natural leaf system showcases the layered structure with varying pore sizes and porosity, inspiring our study. The diagram highlights the cuticle layer with small pores, the epidermis with medium pores, and the mesophyll with large, spongy pores, demonstrating water flow, nutrients, or gases through these layers.

Key properties of membranes crucial for water filtration or purification include permeability, selectivity, mechanical strength, fouling resistance, chemical stability, hydrophilicity, and thermal stability. High permeability ensures efficient water flux, while selectivity enables the removal of specific contaminants. Mechanical strength and chemical stability enhance durability in harsh conditions [62], [63]. Fouling resistance reduces maintenance needs, and hydrophilicity improves wettability and reduces fouling. Thermal stability allows membranes to operate effectively at elevated temperatures. These properties collectively ensure optimal performance and longevity in various water treatment applications. This study will focus on the following performance studies.

First, mechanical durability and robustness of membranes are critical in water filtration applications as they ensure long-term performance and reliability. Membranes

with high mechanical strength can withstand the physical stresses and pressures encountered during filtration processes, reducing the risk of damage and failure[64], [65]. This durability minimizes the need for frequent replacements and maintenance, leading to lower operational costs and increased system efficiency. Robust membranes also maintain their structural integrity under varying environmental conditions, ensuring consistent filtration performance and prolonging the lifespan of the filtration system.[62], [63]

Second, pore size and porosity are essential characteristics they determine filtration efficiency and selectivity by controlling the passage of particles and contaminants. Rapid prototyping of porous morphologies in each layer allows for precise tailoring of these properties, optimizing the membrane's performance for specific applications. [66], [67]Techniques like 3D printing and Direct Ink Writing (DIW) enable the fabrication of complex, multi-layered structures with varied pore sizes and porosity within each layer, mimicking natural systems (Figure 1). This approach enhances the membrane's ability to address different filtration challenges, offering high efficiency, improved durability, and customized functionality in water treatment systems.[68], [69]

Controlling the water contact angle on membrane surfaces is another crucial factor for optimizing their performance in water filtration and purification applications. The water contact angle indicates the hydrophilicity or hydrophobicity of the membrane, which directly affects its wettability, permeability, and fouling resistance. Membranes with a low contact angle (high hydrophilicity) promote better water permeability and reduce the

accumulation of contaminants on the surface, enhancing long-term filtration efficiency. Conversely, hydrophobic membranes with a high contact angle may resist fouling but could impede water flow. Balancing these properties ensures that membranes maintain high performance and durability over extended periods, minimizing maintenance and operational costs. [70], [71]Achieving the ideal water contact angle through surface modifications and material selection is essential for developing advanced membranes tailored to specific filtration needs.

2 MATERIALS AND METHODS

2.1 Materials and Material Selection Rationale

Polyvinylidene fluoride (PVDF) powder with a molecular weight of 534 kDa was sourced from Solvay Specialty. Dimethylacetamide (DMAc) with a purity of ≥99.8% (CAS# 127-19-5) was used as the solvent. The process involved using polyethylene glycol 1000 (PEG 1000) with an average molecular weight of 950–1050 g/mol (CAS# 25322-68-3) as a pore-forming agent and viscosity modifier. Additionally, cellulose acetate (CA) with a molecular weight of 30,000 g/mol was purchased from Sigma Aldrich. The membranes underwent phase inversion using deionized water obtained from the laboratory facility.

The materials used for PVDF composites in this study include polyethylene glycol (PEG) and cellulose acetate (CA). PEG, being hydrophilic, enhances membrane selectivity and serves as an effective pore-forming agent, contributing to improved filtration performance. CA, a prominent cellulose derivative, is derived from natural and renewable resources, offering significant advantages such as low toxicity, biodegradability, and environmental friendliness. CA's inherent hydrophilic groups (–OH) further enhance its filtration capabilities, making CA membranes highly suitable for water treatment and filtration applications. These properties contribute to efficient water permeability and fouling resistance, making PEG and CA ideal components for developing advanced membranes.

2.2 Ink Preparations for DIW

The PVDF, PEG, and CA were combined in a DMAc solution and continuously stirred at 150 rpm for 24 hours at 90°C using a magnetic stirrer. Once fully dissolved, the solutions underwent 30 minutes of sonication to ensure thorough dispersion of CA particles and uniform viscosity. The overall solute concentration was maintained at 20 wt% to achieve thixotropic ink behavior and ensure solvent dispersion homogeneity. The solution was subsequently transferred to a vacuum chamber to eliminate any trapped bubbles that formed during stirring. Afterward, the solution was carefully loaded into syringes, taking care to avoid introducing air bubbles that could create voids during the printing process. Table 2 details the ink compositions, their designations, and the 3D printing parameters utilized.

2.3 DIW 3D Printing of Membranes

A Hyrel SR printer was used to produce single-layer circular films measuring 86 mm in diameter and ranging in thickness from 190 µm to 240 µm. These films were printed onto a clean glass substrate. The printing process employed a nozzle guided by G-codes to ensure precise extrusion control, maintaining a printing speed of 40 mm/s and an extrusion pressure ranging from 5 to 8 psi across all compositions. Throughout the printing process, the substrate and nozzle temperatures remained constant at 23 °C. Following printing, the

glass substrate underwent a 30-minute immersion in deionized (DI) water to initiate phase inversion—a crucial step that solidifies the membrane structure and removes residual solvents. The circular films were used to evaluate contact angle and membrane morphology, while rectangular specimens were designated for tensile testing to assess mechanical properties. These printed membranes promote uniformity in the filtration and are well-suited for applications in microfiltration and water treatment.

Table 2. Nomenclature of prepared membrane samples from 3D printing and their compositions, where T is temperature, P is pressure and t is the thickness of printed membranes

Samples	Membrane compositions			3D printing					
	PVDF (wt.%)	PEG (wt.%)	CA (wt%)	DMAc (Solvent in ml)	T (°C)	P (psi)	Speed (mm/s)	Nozzle (mm)	t (μm)
14PVDF/4PEG/2CA	14	4	2	20	30	6±1	40	0.26	200±10
12PVDF/4PEG/4CA	12	4	4	20					200±20
8PVDF/4PEG/4CA	8	4	8	20					200±30
4PVDF/4PEG/12CA	4	4	12	20					200±15
2PVDF/4PEG/14CA	2	4	14	20					200±20

2.4 Membrane Characterization

2.4.1 Rheology-Membrane Printability

The evaluation of membrane printability included a thorough analysis of the viscosity of each solution. Viscosity measurements were conducted using a 25 mm parallel plate rheometer equipped with a Peltier plate (Discover hybrid rheometer HR30, TA Instruments). The viscoelastic properties of PVDF-PEG-CA were examined at room temperature.

2.4.2 Membrane Morphology

The membrane structure was examined using scanning electron microscopy (SEM)/Focused Ion Beam (FIB) technology on an Auriga instrument (Zeiss), operating at a voltage of 5kV. Before analysis, samples were mounted onto SEM stubs using gold tape and sputter-coated with a thin gold film under vacuum conditions. All membranes were dried overnight in a vacuum before preparation for imaging. Surface porosity and cross-section images were processed using ImageJ software. Surface area and pore volume were determined using adsorption-desorption isotherms analyzed by the Brunauer−Emmett−Teller (BET) method, conducted with a Micromeritics ASAP2420 instrument using Silica Alumina as the reference material (BET Surface Area = 200 ± 6 m^2/g, Total Pore Volume for Adsorption Isotherm: 0.415500 cm^3/g, Total Pore Volume for Desorption Isotherm: 0.575622 cm^3/g). All samples underwent degassing overnight at room temperature before analysis.

2.4.3 Tensile Test for Mechanical Properties

To conduct tensile testing, specimens measuring 0.5 × 4 cm^2 were cut from the circular membranes produced using the DIW process. The mechanical properties of the membranes were assessed through tensile testing using a Discovery HR-30 hybrid rheometer (TA Instruments Inc., USA). A consistent linear strain rate of 30 μm/s was applied to the membranes printed with various concentrations. Multiple samples (5-7) of

each membrane composition were tested to determine mechanical parameters such as Young's modulus, tensile strength, and elongation at break.

2.4.4 Contact Angle

The water contact angle was determined using an SDC350 Integral tilt-type contact angle measuring instrument from SIDIN company, operating under standard room temperature and pressure conditions. De-ionized water served as the probe liquid for all measurements. To enhance accuracy and precision, the contact angle was measured at three random locations on each sample, and the average value was recorded.

3 RESULTS AND DISCUSSIONS

3.1 Membrane 3D Printing via DIW

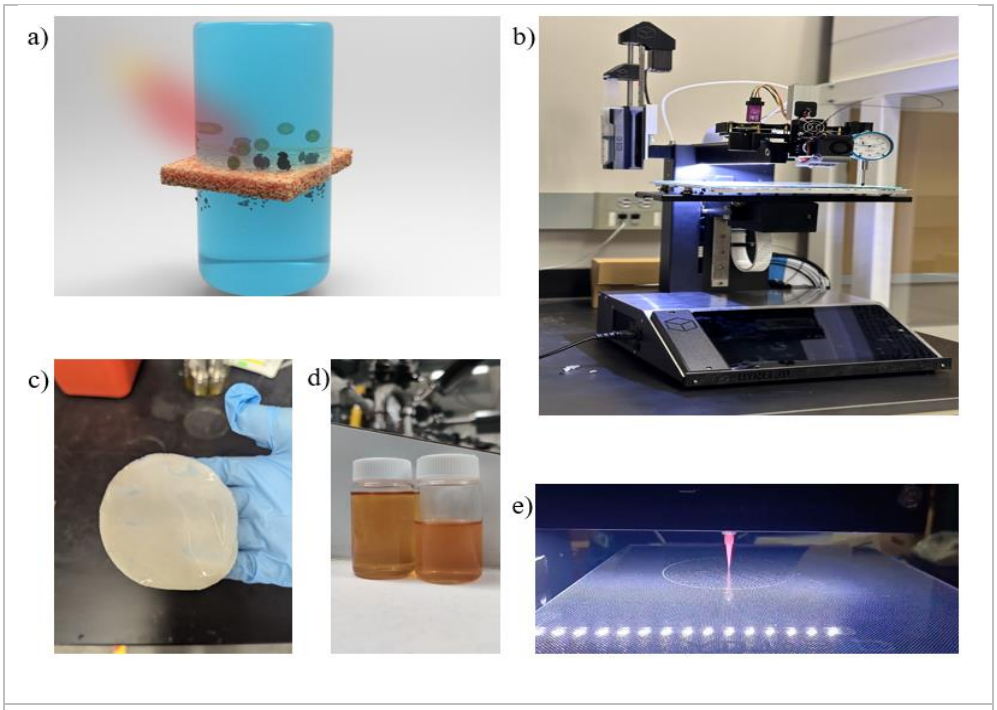

Figure 2. a) Schematic representation of membrane filtration using the membranes fabricated b) DIW setup used c) membranes printed after phase inversion d) Inks used for DIW e)DIW printing process

Membrane 3D printing using Direct Ink Writing (DIW) is pivotal due to its capability to finely control printing parameters, ensuring precise membrane architecture and performance. By manipulating factors like printing speed, extrusion pressure, and nozzle geometry, DIW allows for tailored adjustments in membrane porosity, thickness, and mechanical strength. This control is essential for optimizing membrane properties such as pore size distribution and surface morphology, which directly impact filtration efficiency and durability. Moreover, DIW enables the incorporation of multiple materials like PVDF,

PEG, and CA, enhancing membrane hydrophilicity and overall functionality. Consequently, mastering these printing parameters in DIW not only ensures the reproducibility and reliability of membrane fabrication but also unlocks the potential to design membranes with customized properties tailored to specific industrial and environmental applications.

Figure 2a illustrates the overall functionality of the membranes fabricated which are used for filtration and water treatment purposes. The membranes are designed to selectively allow water molecules to pass through while blocking contaminants and impurities. This ensures efficient filtration, improving water quality and safety for various applications. Figure 2b depicts the DIW setup utilized for 3D printing PVDF/PEG/CA membranes. The process involved adjusting ink compositions while maintaining a printing speed of 40 mm/s at room temperature. Air pressure between 5 and 7 psi assisted in extrusion, with nozzle airflow variability addressed. Initially, achieving consistent prints posed challenges due to composition variations and inadequate pressure control with a mechanical extruder. To address this, a fluid dispenser was implemented to ensure stable air pressure of ~6 psi with a standard deviation of ±1 psi, ensuring uniform ink extrusion. To optimize flow dynamics and improve print quality, a tapered nozzle was used. This nozzle geometry adjustment enabled consistent and precise ink deposition, crucial for maintaining desired membrane thickness and uniformity. More importantly, this design facilitated smoother and more controlled ink flow by reducing the cross-sectional area towards the tip, increasing flow velocity, and minimizing clogging. Ink flow dynamics

were influenced by the interaction between air pressure and the tapered nozzle design, which accelerated ink flow, enhancing control and reducing shear forces that could distort or inconsistently extrude ink. Controlled flow dynamics were essential for maintaining membrane structure integrity during printing.

During the DIW process, 8.6 cm diameter circular films were printed with a positional resolution of 1 μm. Precise pressure control and optimized nozzle flow dynamics enabled the production of membranes with uniform geometry crucial for this membrane study. Figure 2c shows the final membranes post-phase inversion, Figure 2d illustrates the inks used during the printing and process and Figure 2e illustrates the membrane printing process. Phase inversion involved immersing printed membranes in deionized (DI) water, a critical step for membrane formation that solidified membrane structure by removing residual solvents and inducing phase separation between polymer and solvent. During this process, the immersion in DI water transitions the membranes from a liquid to a solid state, triggering the extraction of solvents and causing the polymer to coagulate and form a robust, porous matrix. DI water phase inversion resulted in well-defined porous structures suitable for filtration applications, optimizing membranes for various performance assessments. This process facilitated the development of membranes with enhanced structural integrity and tailored properties, meeting requirements for efficient water treatment. The uniform phase separation ensured by DI water immersion is essential for producing high-performance membranes tailored for effective water filtration and treatment applications.

3.2 Ink Formulation and Rheology

3.2.1 Flow Sweep Test

The viscosity curves shown in Figure 3 illustrate the relationship between viscosity and shear rate for various PVDF/PEG/CA compositions, providing insights into their 3D printing capabilities. Viscosity is a critical parameter in DIW as it influences the flow behavior of the ink through the nozzle, impacting print quality and precision.

The graph shows that all compositions exhibit shear-thinning behavior, where the viscosity decreases with increasing shear rate. This characteristic is essential for DIW, as it allows the ink to flow easily through the nozzle under applied stress while maintaining a higher viscosity at rest to ensure shape retention and stability post-extrusion. Among all samples, the 12PVDF/4PEG/4CA composition shows the highest initial viscosity, starting around 800 Pa.s at low shear rates and decreasing significantly as the shear rate increases. This high initial viscosity suggests that this composition may offer better shape fidelity and less sagging or deformation during printing, but it may require higher extrusion pressures. In contrast, the 2PVDF/4PEG/14CA and 8PVDF/4PEG/4CA compositions have lower viscosities across all shear rates, indicating easier flow through the nozzle but potentially less shape stability. The 14PVDF/4PEG/2CA compositions demonstrate intermediate viscosity profiles, balancing between easy flow and adequate shape retention. This balance is crucial for achieving high-resolution prints with minimal defects.

Overall, the viscosity data suggest that compositions combining manageable flow properties with sufficient post-extrusion stability. This analysis highlights the importance of tuning polymer concentrations to optimize the rheological properties for successful 3D printing applications.

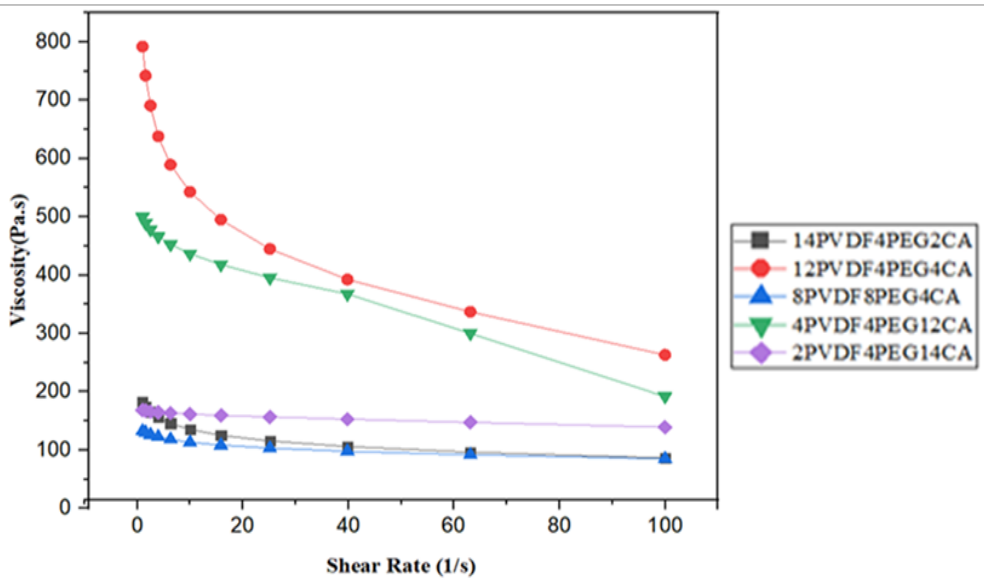

Figure 3. Flow sweep data for the specimens for the viscosity vs. shear rate relationships.

3.2.2 Amplitude Sweep Test

In the amplitude sweep test, the storage modulus (G') and loss modulus (G") were measured across increasing oscillatory strains from 0.999832% to 99.8618% to understand

the viscoelastic behavior of the inks for DIW 3D printing. Ink 1 (14PVDF/4PEG/2CA) starts with G' of 131.546 Pa and G" of 736.268 Pa, decreasing to 77.6794 Pa and 718.35 Pa, respectively. The higher initial loss modulus compared to the storage modulus indicates that Ink 1 exhibits more viscous behavior, which may lead to insufficient shape retention post-extrusion. This fluid-like behavior could cause the ink to spread on the substrate, but given the minimal thickness in 2D film applications, this characteristic might still be favorable.

Ink 2 (12PVDF/4PEG/4CA) shows the highest initial moduli, with G' at 808.787 Pa and G" at 3313.78 Pa, dropping to 390.249 Pa and 2852.23 Pa. These high initial values reflect robust elastic and viscous properties due to higher CA content, enhancing hydrogen bonding and intermolecular interactions. Despite the drop at higher strains, the initial high storage modulus supports structural integrity post-deposition, which is essential for maintaining shape in membranes.

Ink 3 (8PVDF/4PEG/8CA) begins with lower moduli, G' at 64.7056 Pa and G" at 624.093 Pa, decreasing to 35.8667 Pa and 579.693 Pa. The lower moduli indicate a more fluid-like behavior, enhancing extrudability but potentially compromising post-printing stability. The low initial storage modulus suggests limited shape retention, which could be problematic even for 2D film applications like single-layered membranes. Ink 4 (4PVDF/4PEG/12CA) has intermediate values, with G' at 232.512 Pa and G" at 2369.93 Pa, decreasing to 132.055 Pa and 2239.79 Pa. This indicates moderate network strength at

low strains, with higher CA content enhancing flexibility and hydrogen bonding. As strain increases, the ink becomes more fluid-like, balancing extrusion ease and structural integrity, which is beneficial for printing thin films with some level of structural fidelity. Ink 5 (2PVDF/4PEG/14CA) shows the lowest initial moduli, with G' at 34.3414 Pa and G" at 885.631 Pa, dropping to 20.0855 Pa and 870.688 Pa. This predominantly fluid-like behavior, even at low strains, is due to high PEG content acting as a plasticizer, disrupting the PVDF network and enhancing chain mobility. This results in high extrudability but poor shape retention post-deposition, which might be acceptable for very thin films but could be problematic for maintaining precise patterns.

Overall, the decreasing trend in both storage and loss moduli with increasing strain b) ll inks indicates a transition from more solid-like to more fluid-like behavior. For DIW, especially in 2D film applications with minimal thickness, the fluid-like behavior ensures the inks can be easily extruded under high shear. However, maintaining sufficient viscosity to retain shape once deposited is crucial. The varying initial moduli and their reductions highlight the influence of PVDF, PEG, and CA concentrations on viscoelastic properties. Higher PVDF enhances network strength, higher CA promotes elasticity and bonding, and higher PEG reduces viscosity and enhances flow. This interplay allows tailoring inks for optimal printability and structural stability in DIW applications, particularly for creating thin films.

a)

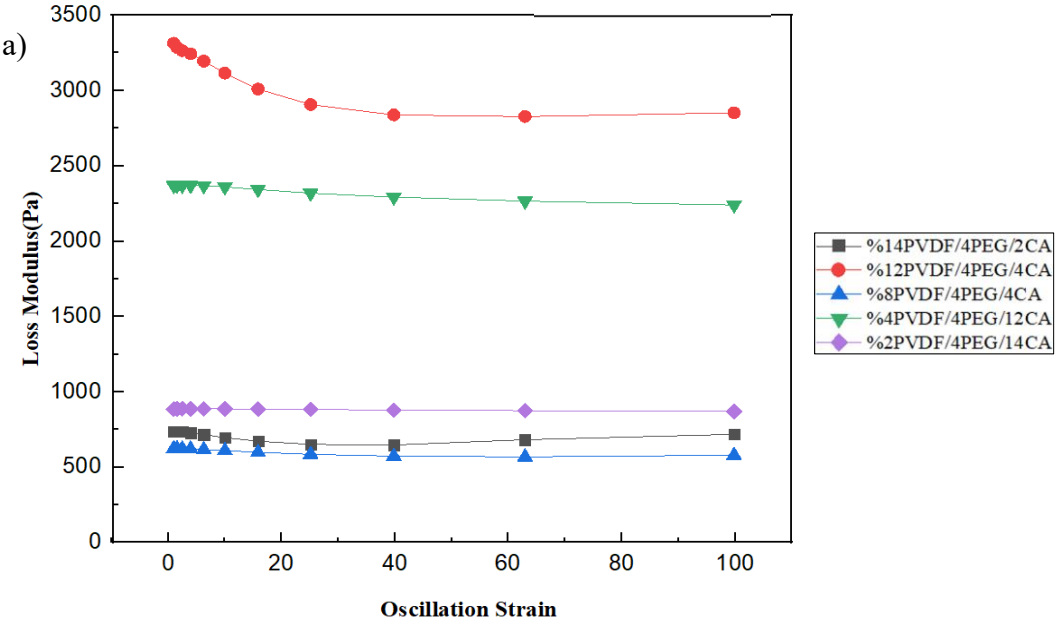
Loss Modulus(Pa)
Oscillation Strain
%14PVDF/4PEG/2CA
%12PVDF/4PEG/4CA
%8PVDF/4PEG/4CA
%4PVDF/4PEG/12CA
%2PVDF/4PEG/14CA

b)

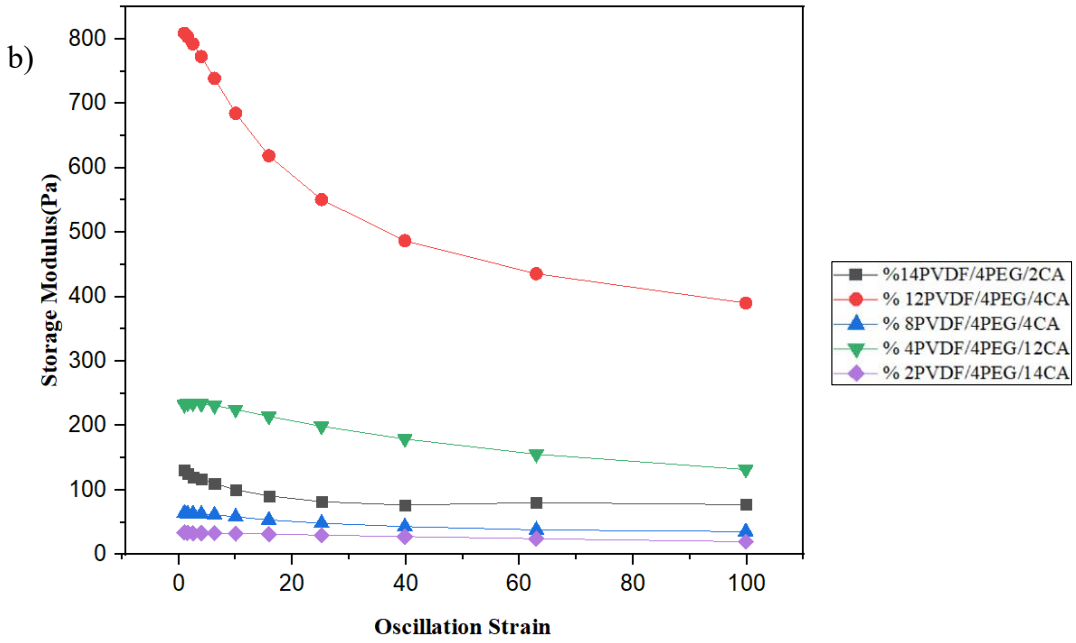
Storage Modulus(Pa)
Oscillation Strain
%14PVDF/4PEG/2CA
% 12PVDF/4PEG/4CA
% 8PVDF/4PEG/4CA
% 4PVDF/4PEG/12CA
% 2PVDF/4PEG/14CA

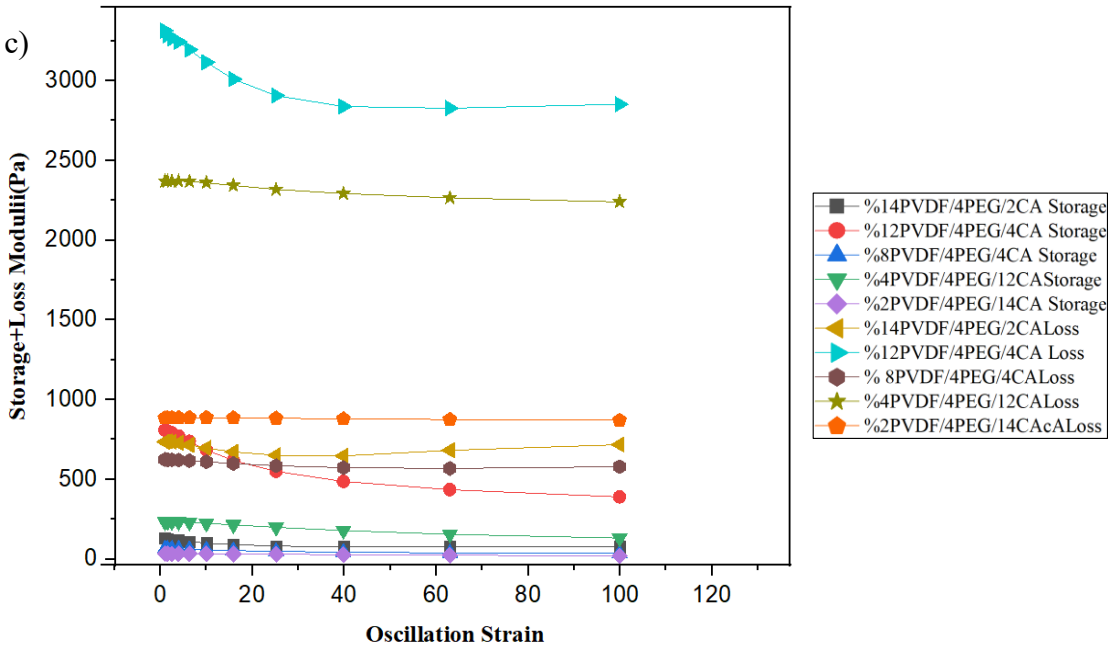

Figure 4. a) Variation of loss modulus concerning oscillation strain for various inks. b) Variation of storage modulus concerning oscillation strain for various inks. c) Comparison of loss and storage moduli for various inks used in the study.

3.2.3 Frequency Sweep Test

In the frequency sweep test, the storage modulus (G') and loss modulus (G") were measured across a range of angular frequencies to assess the viscoelastic behavior of various inks for DIW 3D printing. Ink 1 (14PVDF/4PEG/2CA) demonstrates a transition from elastic to viscous behavior as frequency decreases. At 100 rad/s, G' (3921.08 Pa) is lower than G" (8736.01 Pa), indicating dominant viscous behavior. At 0.1 rad/s, both

moduli drop sharply (G' = 8.6761 Pa, G" = 21.9943 Pa), with G" remaining higher. This fluid-like behavior at lower frequencies ensures smooth extrusion, which is suitable for single-layered 2D membranes despite the higher loss modulus.

Ink 2 (12PVDF/4PEG/4CA) starts with high values at 100 rad/s (G' = 15892.2 Pa, G" = 29380.5 Pa), with G" higher than G' across all frequencies. At 0.1 rad/s, G' and G" decrease to 27.6147 Pa and 91.72 Pa, respectively, indicating a transition from semi-solid-like to more liquid-like behavior. This supports controlled extrusion and sufficient structural integrity for single-layered applications. Ink 3 (8PVDF/4PEG/8CA) exhibits predominant viscous behavior, with G" (9036.56 Pa) much higher than G' (1213.3 Pa) at 100 rad/s. This trend continues with decreasing moduli at lower frequencies (G" = 15.2527 Pa, G' = 2.37729 Pa), highlighting the ink's fluid nature, which facilitates easy flow through the nozzle and is adequate for single-layered membrane printing.

Ink 4 (4PVDF/4PEG/12CA) shows high initial moduli at 100 rad/s (G' = 9105.4 Pa, G" = 33808.7 Pa), with G" dominating. As frequency decreases, both moduli decline (G' = 1.08079 Pa, G" = 53.9444 Pa), indicating fluid readiness for smooth extrusion. This ink's behavior ensures that it flows well through the nozzle and maintains some structural stability, which is acceptable for thin 2D membranes. Ink 5 (2PVDF/4PEG/14CA) has the lowest initial moduli at 100 rad/s (G' = 200.498 Pa, G" = 15856.5 Pa), with G" consistently higher. At 0.1 rad/s, G' and G" reduce to 0.705773 Pa and 19.1631 Pa, indicating predominantly viscous behavior. This facilitates extrusion but requires careful handling to prevent post-deposition deformation due to weaker elastic properties.

a)

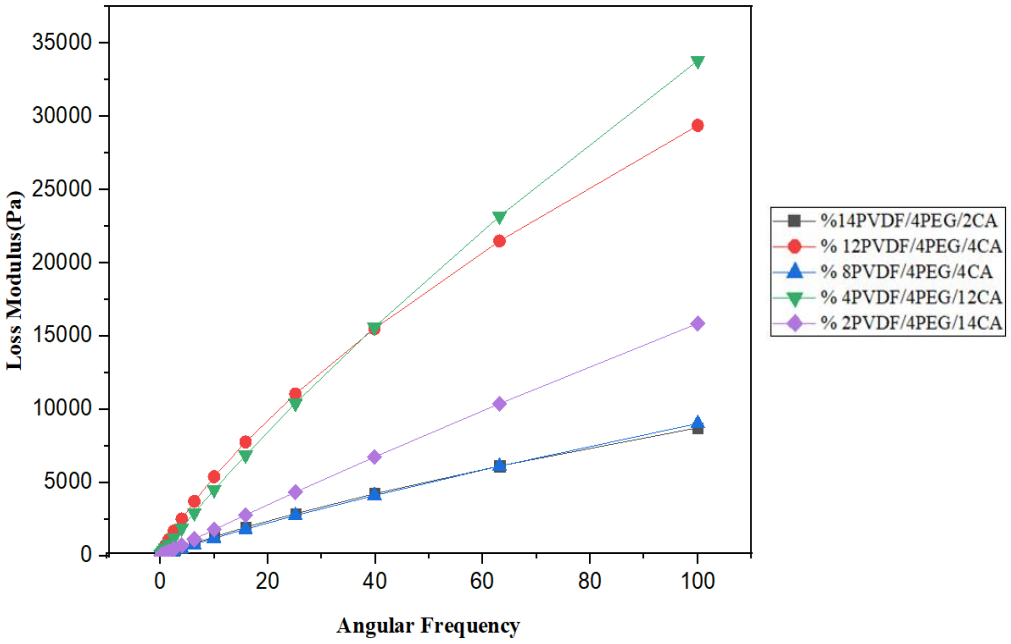
Loss Modulus(Pa)
Angular Frequency
%14PVDF/4PEG/2CA
% 12PVDF/4PEG/4CA
% 8PVDF/4PEG/4CA
% 4PVDF/4PEG/12CA
% 2PVDF/4PEG/14CA

b)

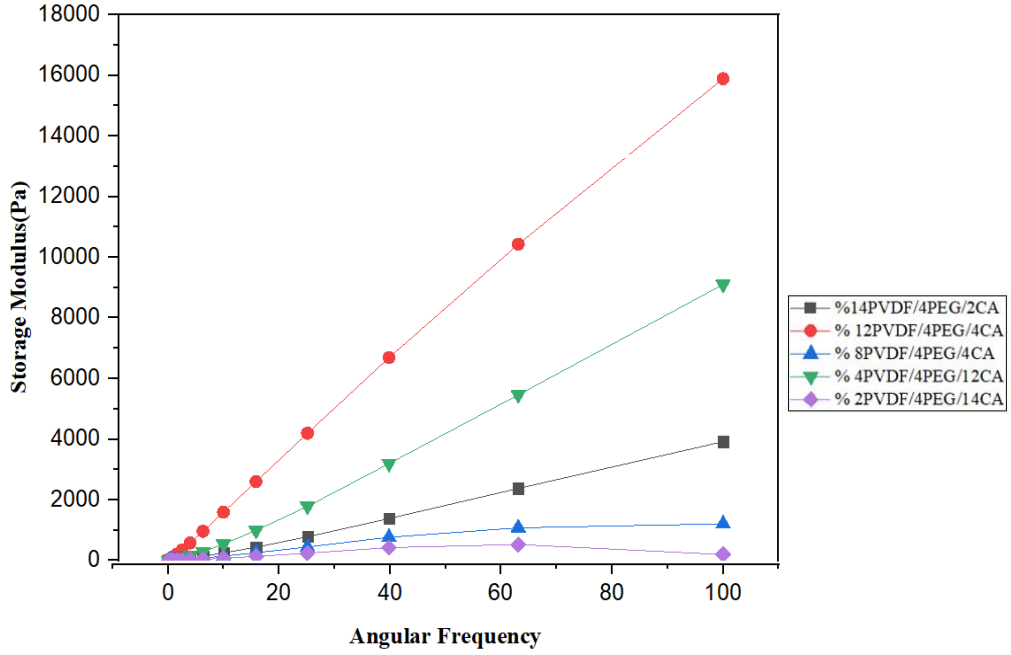
Storage Modulus(Pa)
Angular Frequency
%14PVDF/4PEG/2CA
% 12PVDF/4PEG/4CA
% 8PVDF/4PEG/4CA
% 4PVDF/4PEG/12CA
% 2PVDF/4PEG/14CA

c)

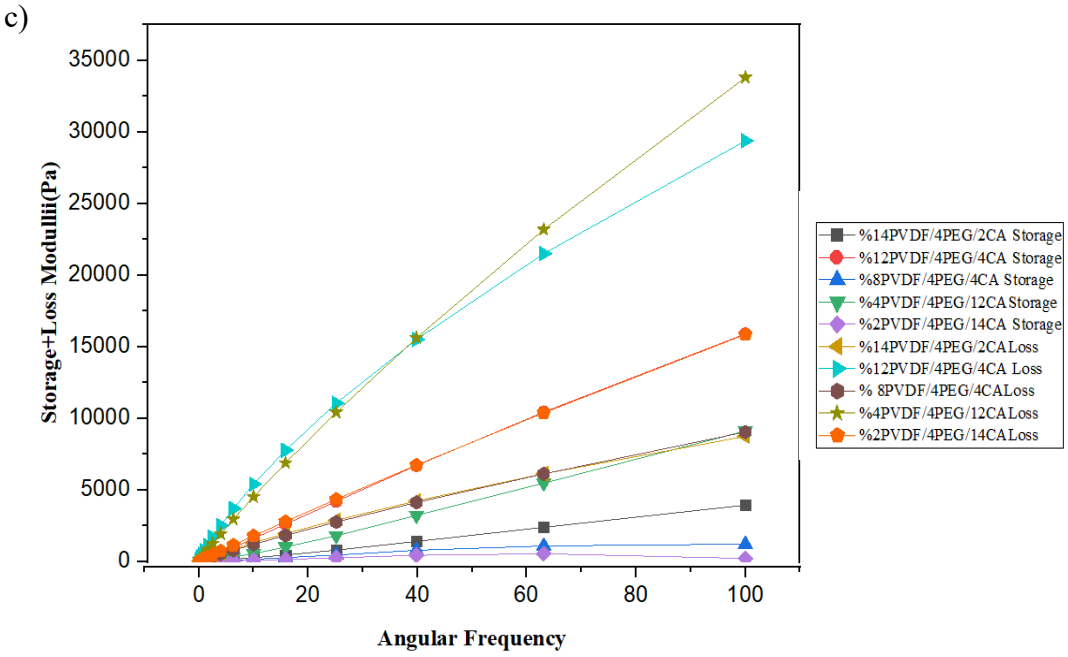

Figure 5. a) Variation of loss modulus with angular frequency for various inks. b) Variation of storage modulus with angular frequency for various inks. c) Comparison of loss and storage moduli with angular frequency for various inks used in the study.

3.3 Morphology and Porosity Studies

The detailed morphological analysis of the PVDF/CA composite membranes, supported by SEM, provides significant insights into their structure and properties. The SEM images in Figure 6 illustrate the morphological characteristics of the PVDF/PEG/CA membranes with varying PVDF/CA concentrations.

The concentration of PVDF in DMAc significantly influences the pore size and porosity of membranes. Higher concentrations of PVDF generally lead to denser membranes with smaller pore sizes, while lower PVDF concentrations result in membranes with larger pores and higher porosity. Previous studies have demonstrated this relationship.

For instance, an investigation into PVDF membranes prepared via phase inversion showed that increasing PVDF concentration in DMAc results in a denser polymer network, thereby reducing the pore size and overall porosity. This is because higher PVDF concentrations enhance the viscosity of the casting solution, which slows down the phase inversion process, leading to a more compact membrane structure with fewer and smaller pores. Conversely, lower PVDF concentrations facilitate faster phase inversion due to lower solution viscosity, resulting in larger pores and higher porosity. This is particularly beneficial for applications requiring high permeability, such as microfiltration and ultrafiltration.

As shown in Figure 6, at 14 wt% PVDF, the membrane shows a dense and tightly packed structure with limited porosity. At 12 wt% PVDF, the membrane exhibits a slight increase in porosity with more noticeable interconnected pores. The 8 wt% PVDF membrane displays a significantly more open and spongy structure. This trend continues with the 4 wt% PVDF membrane, which shows an even more pronounced porous structure with large, well-defined pores. Finally, the 2 wt% PVDF membrane has the highest porosity, featuring a highly interconnected and spongy network.

The SEM analysis of the PVDF/CA membrane surfaces shows a similarly clear trend of increasing pore size with decreasing PVDF concentration and a CA concentration up to 8wt%. Specifically, at 14 wt% PVDF, the membrane has an average surface pore size of 454±50 nm. When the PVDF concentration is reduced to 12 wt%, the pore size increases to 528±37 nm. This trend continues with the 8 wt% PVDF membrane, which exhibits a significantly larger average pore size of 840±46 nm.

The SEM analysis reveals the significant role of CA in influencing pore size in PVDF membranes. Specifically, at 4 wt% PVDF and 12 wt% CA, the membrane shows a remarkably small average pore size of 55±45 nm. The high CA content slows the phase inversion process due to CA's hydrophilic nature and low miscibility with water, leading to a denser, sponge-like structure with fewer macro voids and smaller pores. However, when the PVDF concentration is further decreased to 2 wt% while increasing CA to 14 wt%, the pore size increases to 110±65 nm. This increase in pore size despite high CA content suggests that at very low PVDF concentrations, the overall lower viscosity of the casting solution and the rapid phase inversion process dominate, resulting in larger pores. Therefore, balancing PVDF and CA concentrations is crucial for controlling pore size, as their interplay determines the final porosity and structure of the membrane. This balance is essential for tailoring membranes to specific applications that require precise pore size control for optimal performance.

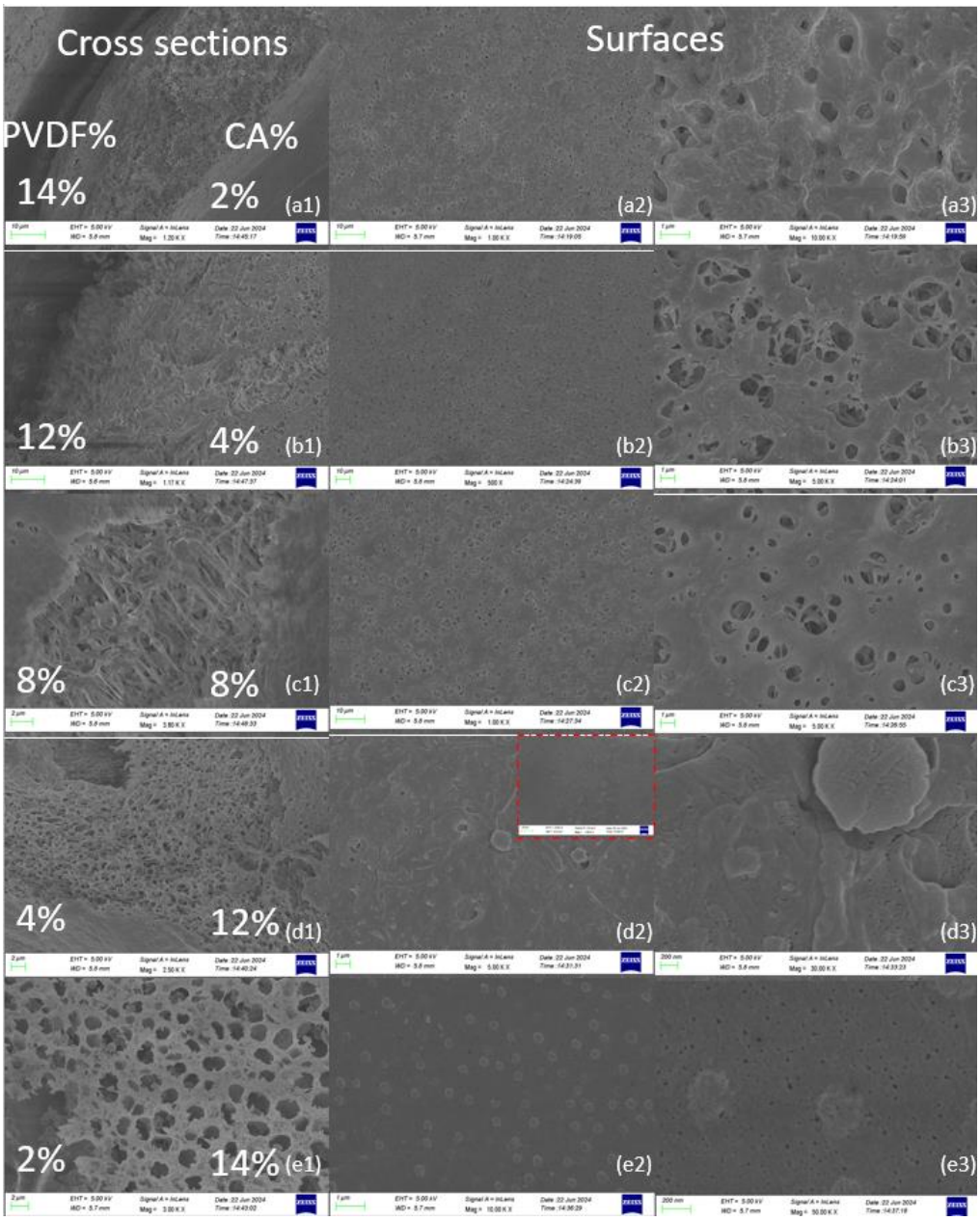

Figure 6. SEM images of the fabricated membranes with varying CA concentrations: (a) 2 wt%, (b) 4 wt%, (c) 8 wt%, (d) 12 wt%, and (e) 14 wt%. Images (a1-e1) depict cross-sections, while images (a2-b2),(a3-b3),(c2-d2),(c3-d3) and (e2-e3) show surface morphologies.

Table 3. Morphological results of fabricated membranes

Sample	SEM	BET	
	Pore size on the surface (nm)	Pore size (nm)	Surface Area (m^2/g)
14PVDF/4PEG/2CA	454±50	5.682	13.285
12PVDF/4PEG/4CA	528±37	5.489	7.261
8PVDF/4PEG/8CA	840±46	5.112	9.316
4PVDF/4PEG/12CA	55±45	4.542	10.194
2PVDF/4PEG/14CA	110±65	5.243	8.591

3.4 Mechanical Characterization of Membranes

The mechanical characterization of the fabricated membranes reveals distinct differences in their properties based on the composition of PVDF, PEG, and CA (Figure 7 & Table 4). The variations in Young's Modulus, elongation at break, and tensile strength (Figure 7 & Table 4) across different membrane formulations reflect the significant influence of these components on mechanical behavior.

For the 14PVDF/4PEG/2CA composition, the membrane shows a relatively low Young's Modulus of 30 MPa, an elongation at break of 15.00%, and a tensile strength of 1.10 MPa (Figure 7 & Table 4). This indicates a moderate balance between stiffness and

flexibility, primarily driven by the high PVDF content, which contributes to the overall structural integrity and flexibility of the membrane. As the CA content increases and PVDF decreases, such as in the 12PVDF/4PEG/4CA membrane, the Young's Modulus drops to 25 MPa, with significant decreases in elongation at break and tensile strength to 4.50% and 0.60 MPa, respectively (Figure 7 & Table 4). This suggests that the initial increase in CA content and reduction in PVDF disrupts the PVDF matrix, resulting in a less stiff and less flexible membrane with lower tensile strength. This is corroborated by SEM images showing a less dense and more porous structure as CA content increases.

Interestingly, the 8PVDF/4PEG/8CA membrane shows a slight increase in Young's Modulus to 31 MPa but maintains low elongation at break (4.34%) and tensile strength (0.75 MPa). This indicates that at this specific ratio, there is a balance between PVDF and CA that allows the membrane to retain some stiffness due to the cohesive interactions between PVDF and CA, despite the increase in porosity shown in SEM images (Figure 7 & Table 4). The most notable change is observed in the 4PVDF/4PEG/12CA membrane, which exhibits a significantly higher Young's Modulus of 85 MPa, elongation at break of 7.03%, and tensile strength of 2.20 MPa (Figure 7 & Table 4). This composition suggests that a higher CA content, despite lower PVDF, can significantly enhance stiffness and tensile strength. The morphological formation, as evident in SEM images, shows a denser and more cohesive polymer network, indicating that the combined effects of ink morphology, printed membrane structure, and higher CA concentrations contribute to a more rigid and robust structure.

Finally, the 2PVDF/4PEG/14CA membrane, despite its high CA content, shows a Young's Modulus of 55 MPa, elongation at break of 4.72%, and tensile strength of 1.00 MPa (Figure 7 & Table 4). This indicates that very high CA content can improve stiffness compared to lower CA concentrations but may not substantially increase tensile strength or elongation. SEM images for this composition reveal a highly porous structure, which can compromise tensile strength and flexibility despite the increased stiffness. Furthermore, higher viscosity indicates a more entangled polymer network in the solution, leading to the formation of denser membranes upon phase inversion. This denser structure is evident in SEM images of membranes with higher CA content. For example, the 12PVDF/4PEG/4CA composition exhibits higher viscosity compared to the 14PVDF/4PEG/2CA composition, correlating with the observed decrease in stiffness and tensile strength due to a less dense polymer network. However, as CA content continues to increase, such as in the 4PVDF/4PEG/12CA and 2PVDF/4PEG/14CA compositions, the high viscosity comparable to the highest viscous ink promotes the formation of a more cohesive and rigid polymer structure, thereby increasing stiffness and tensile strength despite lower PVDF content.

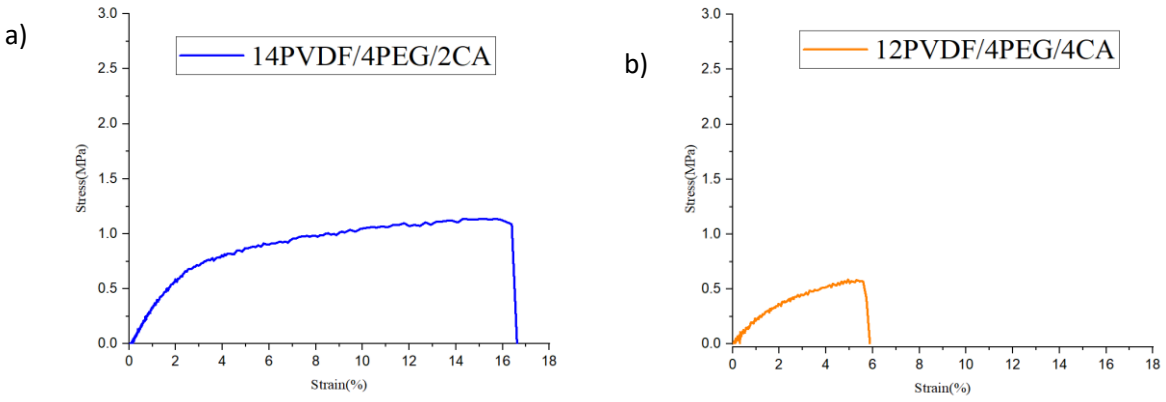

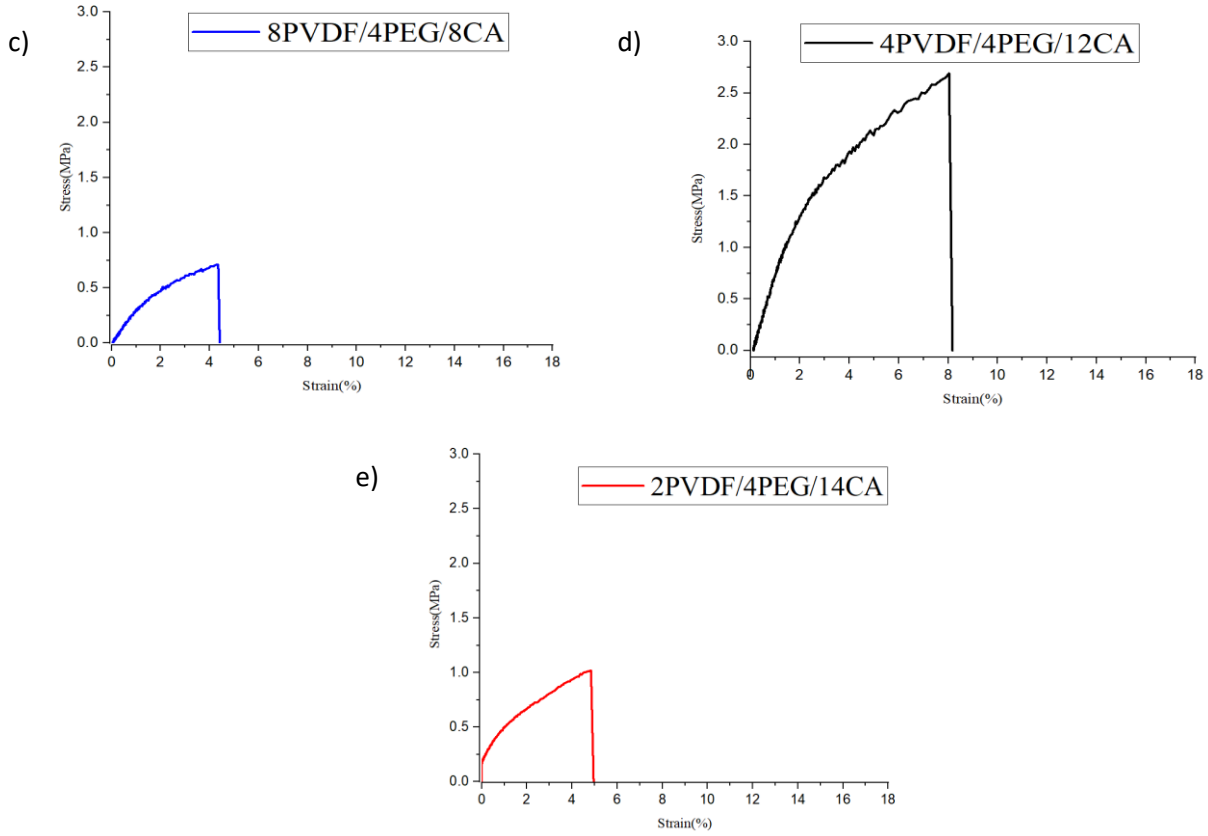

Figure 7. Stress-strain curve relationships of membranes printed in this study namely a) 14PVDF/4PEG/2CA b) 12PVDF/4PEG/4CA c) 8PVDF/4PEG/8CA d) 4PVDF/4PEG/12CA

e) 2PVDF/4PEG/14CA

Table 4. Mechanical Characterization of membranes fabricated

Composition	Young's Modulus (MPa)	Elongation at break (%)	Tensile Strength (MPa)
14PVDF/4PEG/2CA	30±0.02	15.00±1.45	1.10±0.15
12PVDF/4PEG/4CA	25±0.01	4.50±0.85	0.60±0.02
8PVDF/4PEG/8CA	31±0.02	4.34±0.76	0.75±0.03
4PVDF/4PEG/12CA	85±0.30	7.03±1.29	2.20±0.50
2PVDF/4PEG/14CA	55±0.03	4.72±0.64	1.00±0.20

3.5 Contact angle

PVDF is known for its inherent hydrophobicity, which can be reflected by the contact angle measurement with water. Pristine PVDF membranes typically exhibit water contact angles ranging from approximately 81.5° to over 110°, depending on the specific surface treatment and fabrication methods used. Modifications and additives can significantly alter the hydrophilicity of PVDF membranes. For instance, the addition of hydrophilic additives or surface treatments can reduce the contact angle, making the surface more hydrophilic. For example, PEG is known for its significant hydrophilicity, which is reflected in its low water contact angle. Studies have shown that the water contact angle of PEG surfaces can be as low as approximately 20°, indicating a highly hydrophilic surface. This low contact angle is due to the presence of oxygen in the PEG backbone, which promotes strong interactions with water molecules.

In this study, PEG was incorporated as an additive to facilitate pore formation in the PVDF/CA composite membranes. A constant concentration of 4 wt% PEG was used across all samples. The introduction of PEG promotes phase inversion during membrane fabrication, resulting in the formation of larger and more interconnected pores, as suggested in the SEM images shown above. This effect is crucial for improving membrane performance in applications such as filtration and water treatment, where high permeability and effective separation are desired.

CA exhibits a hydrophilic nature, with water contact angles typically lower than 90°, making it less hydrophilic than cellulose but not properly hydrophobic. For example, contact angles for solution-cast CA films are reported to be around 56° to 65°, indicating moderate hydrophilicity. The degree of hydrophilicity can be influenced by the casting conditions and surface treatment, with rougher or patterned surfaces tending to lower the contact angle further, enhancing wettability. Therefore, this study will primarily focus on the influence of CA on the water contact angle of PVDF/PEG/CA membranes. The aim is to understand how varying CA concentrations affect the hydrophilicity and overall performance of the membranes in applications requiring high wettability, such as filtration and water treatment. By analyzing the contact angles, we can determine the optimal balance of CA needed to achieve the desired surface properties. This balance is crucial for tailoring membrane characteristics to meet specific application requirements, ensuring enhanced. The bar graph (Figure 8) illustrates the contact angle measurements for PVDF/PEG/CA membranes with varying concentrations of CA and PVDF. The contact angle is a critical parameter that indicates the wettability of the membrane surface, with lower contact angles

corresponding to higher surface hydrophilicity. As shown in the graph, the contact angles are lowest for the membranes with 8-14 wt% CA, indicating significant hydrophilicity.

For the 12 wt% CA membrane, SEM results indicate a denser and more cohesive polymer network compared to membranes with 8 wt% CA. This increased density reduces porosity and limits the exposure of hydrophilic groups on the surface, which affects the contact angle measurement. Consequently, the 12 wt% CA membrane has a higher contact angle (66.6°) than the 8 wt% CA membrane, indicating decreased hydrophilicity. Similarly, the membrane with 14 wt% CA shows increased surface porosity, allowing more exposure of hydrophilic groups compared to the 12 wt% CA membrane, leading to a lower contact angle. This analysis demonstrates that increasing the CA concentration in PVDF/PEG/CA membranes generally enhances hydrophilicity, and the specific surface porous morphology determines the water contact angles.

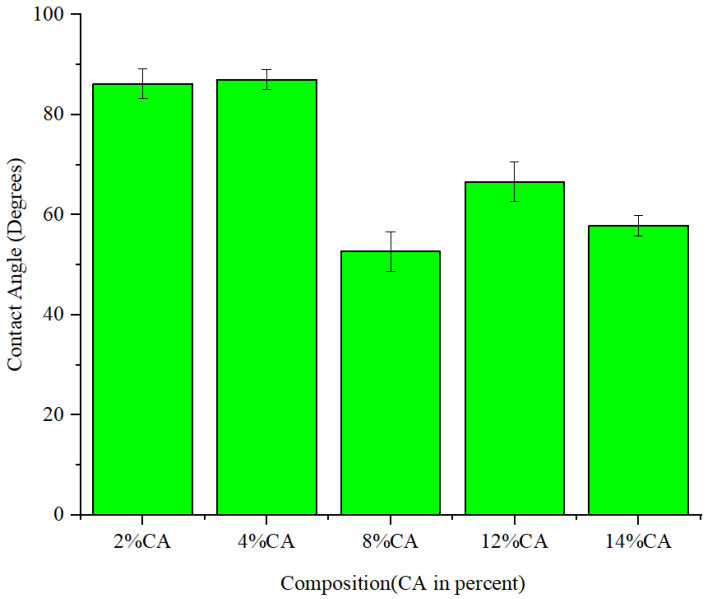

Figure 8. Contact Angle characterization of membranes

4. CONCLUSION

In conclusion, the research demonstrates the significant potential of PVDF based composite membranes fabricated using Direct Ink Writing (DIW) for water treatment applications. The comprehensive characterizations, including rheological analysis, morphological studiess, porosity and mechanical testing, underscore the importance of optimizing the composition of PVDF, PEG, and CA to achieve desired membrane properties. This study highlights the advantages of DIW in producing highly customizable and precise membrane structures, overcoming the limitations associated with traditional fabrication methods. The enhanced properties from these composite membranes could significantly benefit industrial and environmental sectors requiring durable and efficient water treatment solutions. The findings from this research contribute to the knowledge on advanced membrane fabrication techniques and offer promising avenues for future developments in water purification technologies. Further studies may focus on scaling up the production process, exploring fine-tuning of the composite materials, and conducting performance evaluations under various operating conditions.

4 TERMINOLOGY

- CA: Cellulose Acetate; a hydrophilic, biodegradable polymer derived from natural and renewable resources, enhancing membrane hydrophilicity and fouling resistance.
- DIW: Direct Ink Writing; an extrusion-based 3D printing technique allowing precise control over membrane architecture and composition by depositing viscoelastic inks through a fine nozzle.
- DMAc: Dimethylacetamide; a solvent used in the preparation of PVDF, PEG, and CA solutions for DIW membrane fabrication.
- MF: Microfiltration; a membrane filtration process that removes large particles and bacteria from water, typically with pore sizes ranging from 0.1 to 10 micrometers.
- NF: Nanofiltration; a membrane filtration process effective at removing divalent ions, small organic molecules, and certain salts, with pore sizes typically between 0.001 and 0.01 micrometers.
- PEG: Polyethylene Glycol; a hydrophilic polymer used as a pore-forming agent to improve membrane selectivity and enhance hydrophilicity.
- PES: Polyethersulfone; a polymer known for its high mechanical strength and thermal stability, commonly used in ultrafiltration (UF) and nanofiltration (NF) applications.
- PP: Polypropylene; a low-cost, chemically resistant polymer primarily used in microfiltration (MF) applications.

- PSF: Polysulfone; a polymer with high mechanical strength and thermal stability, used in ultrafiltration (UF) and nanofiltration (NF) applications.
- PVDF: Polyvinylidene Fluoride; a semicrystalline polymer widely used in membrane fabrication due to its excellent chemical resistance, thermal stability, and mechanical strength.
- RO: Reverse Osmosis; a membrane filtration process that removes nearly all dissolved salts, organic molecules, and other impurities from water, with pore sizes less than 0.001 micrometers.
- UF: Ultrafiltration; a membrane filtration process that removes bacteria, viruses, and some larger organic molecules from water, with pore sizes generally between 0.01 and 0.1 micrometers.

5 REFERENCES:

[1] J. R. Werber, C. O. Osuji, and M. Elimelech, "Materials for next-generation desalination and water purification membranes," *Nature Reviews Materials 2016 1:5*, vol. 1, no. 5, pp. 1–15, Apr. 2016, doi: 10.1038/natrevmats.2016.18.

[2] W. Guo, H. H. Ngo, and J. Li, "A mini-review on membrane fouling," *Bioresour Technol*, vol. 122, pp. 27–34, Oct. 2012, doi: 10.1016/J.BIORTECH.2012.04.089.

[3] W. J. Lau, A. F. Ismail, N. Misdan, and M. A. Kassim, "A recent progress in thin film composite membrane: A review," *Desalination*, vol. 287, pp. 190–199, Feb. 2012, doi: 10.1016/J.DESAL.2011.04.004.

[4] M. Elimelech and W. A. Phillip, "The future of seawater desalination: Energy, technology, and the environment," *Science (1979)*, vol. 333, no. 6043, pp. 712–717, Aug. 2011, doi: 10.1126/SCIENCE.1200488/SUPPL_FILE/ELIMELECH.SOM.PDF.

[5] X. Lu and M. Elimelech, "Fabrication of desalination membranes by interfacial polymerization: history, current efforts, and future directions," *Chem Soc Rev*, vol. 50, no. 11, pp. 6290–6307, Jun. 2021, doi: 10.1039/D0CS00502A.

[6] I. Shahonya, F. Nangolo, M. Erinosho, and E. Angula, "Scaling and Fouling of Reverse Osmosis (RO) Membrane: Technical Review," *Lecture Notes in Mechanical Engineering*, pp. 41–47, 2021, doi: 10.1007/978-981-16-3641-7_7.

[7] M. M. Pendergast and E. M. V. Hoek, "A review of water treatment membrane nanotechnologies," *Energy Environ Sci*, vol. 4, no. 6, pp. 1946–1971, Jun. 2011, doi: 10.1039/C0EE00541J.

[8] M. Q. Seah, W. J. Lau, P. S. Goh, H. H. Tseng, R. A. Wahab, and A. F. Ismail, "Progress of Interfacial Polymerization Techniques for Polyamide Thin Film (Nano)Composite Membrane Fabrication: A Comprehensive Review," *Polymers 2020, Vol. 12, Page 2817*, vol. 12, no. 12, p. 2817, Nov. 2020, doi: 10.3390/POLYM12122817.

[9] T. Mohammadi and E. Saljoughi, “Effect of production conditions on morphology and permeability of asymmetric cellulose acetate membranes,” *Desalination*, vol. 243, no. 1–3, pp. 1–7, Jul. 2009, doi: 10.1016/J.DESAL.2008.04.010.

[10] M. Ulbricht, “Advanced functional polymer membranes,” *Polymer (Guildf)*, vol. 47, no. 7, pp. 2217–2262, Mar. 2006, doi: 10.1016/j.polymer.2006.01.084.

[11] A. Abdelrasoul, H. Doan, A. Lohi, A. Abdelrasoul, H. Doan, and A. Lohi, “Fouling in Membrane Filtration and Remediation Methods,” *Mass Transfer - Advances in Sustainable Energy and Environment Oriented Numerical Modeling*, Jul. 2013, doi: 10.5772/52370.

[12] L. Zhong, Y. Wang, D. Liu, Z. Zhu, and W. Wang, “Recent advances in membrane distillation using electrospun membranes: advantages, challenges, and outlook,” *Environ Sci (Camb)*, vol. 7, no. 6, pp. 1002–1019, Jun. 2021, doi: 10.1039/D1EW00128K.

[13] “Recent progress in developing advanced membranes for emulsified oil/water separation - Google Search.” Accessed: Jul. 06, 2024. [Online]. Available: https://www.google.com/search?q=Recent+progress+in+developing+advanced+membranes+for+emulsified+oil%2Fwater+separation&rlz=1C1VIQF_enUS1083US1083&oq=Recent+progress+in+developing+advanced+membranes+for+emulsified+oil%2Fwater+separation&gs_lcrp=EgZjaHJvbWUyBggAEEUYOdIBBzM2MWowajeoAgCwAgA&sourceid=chrome&ie=UTF-8

[14] J. H. Jhaveri and Z. V. P. Murthy, “A comprehensive review on anti-fouling nanocomposite membranes for pressure driven membrane separation processes,” *Desalination*, vol. 379, pp. 137–154, Feb. 2016, doi: 10.1016/j.desal.2015.11.009.

[15] J. Huang, X. Ran, L. Sun, H. Bi, and X. Wu, “Recent advances in membrane technologies applied in oil–water separation,” *Discover Nano*, vol. 19, no. 1, Dec. 2024, doi: 10.1186/S11671-024-04012-W.

[16] J. Huang, X. Ran, L. Sun, H. Bi, and X. Wu, “Recent advances in membrane technologies applied in oil–water separation,” *Discover Nano*, vol. 19, no. 1, Dec. 2024, doi: 10.1186/S11671-024-04012-W.

[17] L. Shi, R. Wang, Y. Cao, C. Feng, D. T. Liang, and J. H. Tay, “Fabrication of poly(vinylidene fluoride-co-hexafluropropylene) (PVDF-HFP) asymmetric microporous hollow fiber membranes,” *J Memb Sci*, vol. 305, no. 1–2, pp. 215–225, Nov. 2007, doi: 10.1016/J.MEMSCI.2007.08.012.

[18] M. G. Buonomenna, P. Macchi, M. Davoli, and E. Drioli, “Poly(vinylidene fluoride) membranes by phase inversion: the role the casting and coagulation conditions play in their morphology, crystalline structure and properties,” *Eur Polym J*, vol. 43, no. 4, pp. 1557–1572, Apr. 2007, doi: 10.1016/J.EURPOLYMJ.2006.12.033.

[19] M. M. R. Abed, S. C. Kumbharkar, A. M. Groth, and K. Li, “Ultrafiltration PVDF hollow fibre membranes with interconnected bicontinuous structures produced via a single-step phase inversion technique,” *J Memb Sci*, vol. 407–408, pp. 145–154, Jul. 2012, doi: 10.1016/J.MEMSCI.2012.03.029.

[20] F. Liu, N. A. Hashim, Y. Liu, M. R. M. Abed, and K. Li, “Progress in the production and modification of PVDF membranes,” *J Memb Sci*, vol. 375, no. 1–2, pp. 1–27, Jun. 2011, doi: 10.1016/J.MEMSCI.2011.03.014.

[21] Z. Cui, E. Drioli, and Y. M. Lee, “Recent progress in fluoropolymers for membranes,” *Prog Polym Sci*, vol. 39, no. 1, pp. 164–198, Jan. 2014, doi: 10.1016/J.PROGPOLYMSCI.2013.07.008.

[22] H. Wu, J. Shi, X. Ning, Y. Z. Long, and J. Zheng, “The High Flux of Superhydrophilic-Superhydrophobic Janus Membrane of cPVA-PVDF/PMMA/GO by Layer-by-Layer Electrospinning for High Efficiency Oil-Water Separation,” *Polymers 2022, Vol. 14, Page 621*, vol. 14, no. 3, p. 621, Feb. 2022, doi: 10.3390/POLYM14030621.

[23] Y. Peng, Y. Dong, H. Fan, P. Chen, Z. Li, and Q. Jiang, “Preparation of polysulfone membranes via vapor-induced phase separation and simulation of direct-contact

membrane distillation by measuring hydrophobic layer thickness," *Desalination*, vol. 316, pp. 53–66, May 2013, doi: 10.1016/J.DESAL.2013.01.021.

[24] J. Yin and B. Deng, "Polymer-matrix nanocomposite membranes for water treatment," *J Memb Sci*, vol. 479, pp. 256–275, Apr. 2015, doi: 10.1016/j.memsci.2014.11.019.

[25] L. Y. Ng, A. W. Mohammad, C. P. Leo, and N. Hilal, "Polymeric membranes incorporated with metal/metal oxide nanoparticles: A comprehensive review," *Desalination*, vol. 308, pp. 15–33, Jan. 2013, doi: 10.1016/j.desal.2010.11.033.

[26] F. Liu, N. A. Hashim, Y. Liu, M. R. M. Abed, and K. Li, "Progress in the production and modification of PVDF membranes," *J Memb Sci*, vol. 375, no. 1–2, pp. 1–27, Jun. 2011, doi: 10.1016/J.MEMSCI.2011.03.014.

[27] G. dong Kang and Y. ming Cao, "Application and modification of poly(vinylidene fluoride) (PVDF) membranes - A review," *J Memb Sci*, vol. 463, pp. 145–165, Aug. 2014, doi: 10.1016/j.memsci.2014.03.055.

[28] S. Zhao, L. Zou, C. Y. Tang, and D. Mulcahy, "Recent developments in forward osmosis: Opportunities and challenges," *J Memb Sci*, vol. 396, pp. 1–21, Apr. 2012, doi: 10.1016/j.memsci.2011.12.023.

[29] J. Huang, X. Ran, L. Sun, H. Bi, and X. Wu, "Recent advances in membrane technologies applied in oil–water separation," *Discover Nano*, vol. 19, no. 1, Dec. 2024, doi: 10.1186/S11671-024-04012-W.

[30] G. Arthanareeswaran, P. Thanikaivelan, K. Srinivasn, D. Mohan, and M. Rajendran, "Synthesis, characterization and thermal studies on cellulose acetate membranes with additive," *Eur Polym J*, vol. 40, no. 9, pp. 2153–2159, Sep. 2004, doi: 10.1016/J.EURPOLYMJ.2004.04.024.

[31] A. Kaiser, W. J. Stark, and R. N. Grass, “Rapid Production of a Porous Cellulose Acetate Membrane for Water Filtration using Readily Available Chemicals,” 2017, doi: 10.1021/acs.jchemed.6b00776.

[32] B. S. Lalia, V. Kochkodan, R. Hashaikeh, and N. Hilal, “A review on membrane fabrication: Structure, properties and performance relationship,” *Desalination*, vol. 326, pp. 77–95, Oct. 2013, doi: 10.1016/J.DESAL.2013.06.016.

[33] J. Nambi Krishnan, K. R. Venkatachalam, O. Ghosh, K. Jhaveri, A. Palakodeti, and N. Nair, “Review of Thin Film Nanocomposite Membranes and Their Applications in Desalination,” *Front Chem*, vol. 10, Jan. 2022, doi: 10.3389/FCHEM.2022.781372/FULL.

[34] J. Teng *et al.*, “A critical review on thermodynamic mechanisms of membrane fouling in membrane-based water treatment process,” *Front Environ Sci Eng*, vol. 17, no. 10, Oct. 2023, doi: 10.1007/S11783-023-1729-6.

[35] X. Lu and M. Elimelech, “Fabrication of desalination membranes by interfacial polymerization: history, current efforts, and future directions,” *Chem Soc Rev*, vol. 50, no. 11, pp. 6290–6307, Jun. 2021, doi: 10.1039/D0CS00502A.

[36] P. S. Goh, T. Matsuura, A. F. Ismail, and N. Hilal, “Recent trends in membranes and membrane processes for desalination,” *Desalination*, vol. 391, pp. 43–60, Aug. 2016, doi: 10.1016/J.DESAL.2015.12.016.

[37] B. Van Der Bruggen, “Chemical modification of polyethersulfone nanofiltration membranes: A review,” *J Appl Polym Sci*, vol. 114, no. 1, pp. 630–642, Oct. 2009, doi: 10.1002/APP.30578.

[38] V. Freger, “Nanoscale heterogeneity of polyamide membranes formed by interfacial polymerization,” *Langmuir*, vol. 19, no. 11, pp. 4791–4797, May 2003, doi: 10.1021/LA020920Q/ASSET/IMAGES/MEDIUM/LA020920QE00002.GIF.

[39] G. Y. Chai and W. B. Krantz, “Formation and characterization of polyamide membranes via interfacial polymerization,” *J Memb Sci*, vol. 93, no. 2, pp. 175–192, Aug. 1994, doi: 10.1016/0376-7388(94)80006-5.

[40] B. H. Jeong *et al.*, “Interfacial polymerization of thin film nanocomposites: A new concept for reverse osmosis membranes,” *J Memb Sci*, vol. 294, no. 1–2, pp. 1–7, May 2007, doi: 10.1016/J.MEMSCI.2007.02.025.

[41] X. Lu and M. Elimelech, “Fabrication of desalination membranes by interfacial polymerization: history, current efforts, and future directions,” *Chem Soc Rev*, vol. 50, no. 11, pp. 6290–6307, Jun. 2021, doi: 10.1039/D0CS00502A.

[42] M. G. Buonomenna, P. Macchi, M. Davoli, and E. Drioli, “Poly(vinylidene fluoride) membranes by phase inversion: the role the casting and coagulation conditions play in their morphology, crystalline structure and properties,” *Eur Polym J*, vol. 43, no. 4, pp. 1557–1572, Apr. 2007, doi: 10.1016/J.EURPOLYMJ.2006.12.033.

[43] D. M. Warsinger, J. Swaminathan, E. Guillen-Burrieza, H. A. Arafat, and J. H. Lienhard V, “Scaling and fouling in membrane distillation for desalination applications: A review,” *Desalination*, vol. 356, pp. 294–313, Jan. 2015, doi: 10.1016/J.DESAL.2014.06.031.

[44] Z. Wang *et al.*, “Nanoparticle-templated nanofiltration membranes for ultrahigh performance desalination,” *Nature Communications 2018 9:1*, vol. 9, no. 1, pp. 1–9, May 2018, doi: 10.1038/s41467-018-04467-3.

[45] W. J. Koros and C. Zhang, “Materials for next-generation molecularly selective synthetic membranes,” *Nature Materials 2017 16:3*, vol. 16, no. 3, pp. 289–297, Jan. 2017, doi: 10.1038/nmat4805.

[46] X. Wang, M. Jiang, Z. Zhou, J. Gou, and D. Hui, “3D printing of polymer matrix composites: A review and prospective,” *Compos B Eng*, vol. 110, pp. 442–458, Feb. 2017, doi: 10.1016/J.COMPOSITESB.2016.11.034.

[47] A. Soo, S. M. Ali, and H. K. Shon, "3D printing for membrane desalination: Challenges and future prospects," *Desalination*, vol. 520, p. 115366, Dec. 2021, doi: 10.1016/J.DESAL.2021.115366.

[48] Z. X. Low, Y. T. Chua, B. M. Ray, D. Mattia, I. S. Metcalfe, and D. A. Patterson, "Perspective on 3D printing of separation membranes and comparison to related unconventional fabrication techniques," *J Memb Sci*, vol. 523, pp. 596–613, Feb. 2017, doi: 10.1016/J.MEMSCI.2016.10.006.

[49] C. Xu, B. Quinn, L. L. Lebel, D. Therriault, and G. L'espérance, "Multi-Material Direct Ink Writing (DIW) for Complex 3D Metallic Structures with Removable Supports," *ACS Appl Mater Interfaces*, vol. 11, no. 8, pp. 8499–8506, Feb. 2019, doi: 10.1021/ACSAMI.8B19986/SUPPL_FILE/AM8B19986_SI_004.AVI.

[50] S. Tagliaferri, A. Panagiotopoulos, and C. Mattevi, "Direct ink writing of energy materials," *Mater Adv*, vol. 2, p. 540, 2021, doi: 10.1039/d0ma00753f.

[51] M. A. S. R. Saadi *et al.*, "Direct Ink Writing: A 3D Printing Technology for Diverse Materials," *Advanced Materials*, vol. 34, no. 28, p. 2108855, Jul. 2022, doi: 10.1002/ADMA.202108855.

[52] Z. He *et al.*, "Direct ink writing of geopolymer-based membranes with anisotropic structures for water treatment," *J Memb Sci*, vol. 685, p. 121953, Nov. 2023, doi: 10.1016/J.MEMSCI.2023.121953.

[53] B. Imtiaz, N. A. Shepelin, P. C. Sherrell, S. E. Kentish, and A. V. Ellis, "Direct ink writing of dehydrofluorinated Poly(Vinylidene Difluoride) for microfiltration membrane fabrication," *J Memb Sci*, vol. 632, p. 119347, Aug. 2021, doi: 10.1016/J.MEMSCI.2021.119347.

[54] S. Li *et al.*, "3D printing of magnetically responsive superhydrophobic porous membranes with on-demand oil-absorption property," *Colloids Surf A Physicochem Eng Asp*, vol. 682, p. 132965, Feb. 2024, doi: 10.1016/J.COLSURFA.2023.132965.

[55] X. Li, H. Shan, W. Zhang, and B. Li, “3D printed robust superhydrophilic and underwater superoleophobic composite membrane for high efficient oil/water separation,” *Sep Purif Technol*, vol. 237, p. 116324, Apr. 2020, doi: 10.1016/J.SEPPUR.2019.116324.

[56] Z. Feng *et al.*, “Nano graphene oxide creates a fully biobased 3D-printed membrane with high-flux and anti-fouling oil/water separation performance,” *Chemical Engineering Journal*, vol. 485, p. 149603, Apr. 2024, doi: 10.1016/J.CEJ.2024.149603.

[57] J. Yuan, C. Yi, H. Jiang, F. Liu, and G. J. Cheng, “Direct Ink Writing of Hierarchically Porous Cellulose/Alginate Monolithic Hydrogel as a Highly Effective Adsorbent for Environmental Applications,” 2021, doi: 10.1021/acsapm.0c01002.

[58] A. Mughal *et al.*, “3D-printed polyether-ether ketone/carboxymethyl cellulose scaffolds coated with Zn–Mn doped mesoporous bioactive glass nanoparticles,” *J Mech Behav Biomed Mater*, vol. 156, p. 106581, Aug. 2024, doi: 10.1016/J.JMBBM.2024.106581.

[59] Y. Zheng, H. Zhang, Z. Wang, A. Lu, A. Yu, and B. Duan, “Chitin nanofibrils assisted 3D printing all-chitin hydrogels for wound dressing,” *Carbohydr Polym*, vol. 334, p. 122028, Jun. 2024, doi: 10.1016/J.CARBPOL.2024.122028.

[60] S. G. Marapureddy *et al.*, “Rheology and direct write printing of chitosan - graphene oxide nanocomposite hydrogels for differentiation of neuroblastoma cells,” *Carbohydr Polym*, vol. 269, p. 118254, Oct. 2021, doi: 10.1016/J.CARBPOL.2021.118254.

[61] H. Baniasadi, R. Ajdary, J. Trifol, O. J. Rojas, and J. Seppälä, “Direct ink writing of aloe vera/cellulose nanofibrils bio-hydrogels,” *Carbohydr Polym*, vol. 266, p. 118114, Aug. 2021, doi: 10.1016/J.CARBPOL.2021.118114.

[62] P. S. Goh, T. Matsuura, A. F. Ismail, and N. Hilal, "Recent trends in membranes and membrane processes for desalination," *Desalination*, vol. 391, pp. 43–60, Aug. 2016, doi: 10.1016/J.DESAL.2015.12.016.

[63] M. Elimelech and W. A. Phillip, "The future of seawater desalination: Energy, technology, and the environment," *Science (1979)*, vol. 333, no. 6043, pp. 712–717, Aug. 2011, doi: 10.1126/SCIENCE.1200488/SUPPL_FILE/ELIMELECH.SOM.PDF.

[64] R. W. Baker, "Membrane Technology and Applications," *Membrane Technology and Applications*, Jul. 2012, doi: 10.1002/9781118359686.

[65] M. Ulbricht, "Advanced functional polymer membranes," *Polymer (Guildf)*, vol. 47, no. 7, pp. 2217–2262, Mar. 2006, doi: 10.1016/J.POLYMER.2006.01.084.

[66] Y. Liang *et al.*, "Polyamide nanofiltration membrane with highly uniform sub-nanometre pores for sub-1 Å precision separation," *Nature Communications 2020 11:1*, vol. 11, no. 1, pp. 1–9, Apr. 2020, doi: 10.1038/s41467-020-15771-2.

[67] L. Eykens, K. De Sitter, C. Dotremont, L. Pinoy, and B. Van der Bruggen, "Membrane synthesis for membrane distillation: A review," *Sep Purif Technol*, vol. 182, pp. 36–51, Jul. 2017, doi: 10.1016/J.SEPPUR.2017.03.035.

[68] R. Online *et al.*, "Graphene/PVDF flat-sheet membrane for the treatment of RO brine from coal seam gas produced water by air gap membrane distillation Publication Details", Accessed: Jul. 10, 2024. [Online]. Available: http://ro.uow.edu.au/eispapers/5771

[69] M. A. Shannon, P. W. Bohn, M. Elimelech, J. G. Georgiadis, B. J. Marĩas, and A. M. Mayes, "Science and technology for water purification in the coming decades," *Nature 2008 452:7185*, vol. 452, no. 7185, pp. 301–310, Mar. 2008, doi: 10.1038/nature06599.

[70] F. E. Ahmed, B. S. Lalia, and R. Hashaikeh, “A review on electrospinning for membrane fabrication: Challenges and applications,” *Desalination*, vol. 356, pp. 15–30, Jan. 2015, doi: 10.1016/J.DESAL.2014.09.033.

[71] A. Manmadhachary, R. Tulasi, and P. Chattoraj, “3D-Printed membrane for water treatment,” *3D Printing Technology for Water Treatment Applications*, pp. 133–156, Jan. 2022, doi: 10.1016/B978-0-323-99861-1.00007-2.